Title

Optineurin tunes outside-in signaling to regulate lysosome biogenesis and phagocytic clearance in the retina

Journal

Current Biology, 33(18)

ISSN

0960-9822

Authors

Tan, Li Xuan
Germer, Colin J
Thamban, Thushara
et al.

Publication Date

2023-09-01

DOI

10.1016/j.cub.2023.07.031

Peer reviewed

HHS Public Access

Author manuscript

Curr Biol. Author manuscript; available in PMC 2024 September 25.

Published in final edited form as:

Curr Biol. 2023 September 25; 33(18): 3805–3820.e7. doi:10.1016/j.cub.2023.07.031.

Optineurin tunes outside-in signaling to regulate lysosome biogenesis and phagocytic clearance in the retina

Li Xuan Tan[1], **Colin J. Germer**[1,2], **Thushara Thamban**[1], **Nilsa La Cunza**[1,2], **Aparna Lakkaraju**[1,2,3,4,*]

[1]Department of Ophthalmology, School of Medicine, University of California, San Francisco, San Francisco, CA 94143, USA.

[2]Pharmaceutical Sciences and Pharmacogenomics Graduate Program, University of California, San Francisco, San Francisco, CA 94143, USA.

[3]Department of Anatomy, School of Medicine, University of California, San Francisco, San Francisco, CA 94143, USA.

Summary

Balancing the competing demands of phagolysosomal degradation and autophagy is a significant challenge for phagocytic tissues. Yet, how this plasticity is accomplished in health and disease is poorly understood. In the retina, circadian phagocytosis and degradation of photoreceptor outer segments by the postmitotic retinal pigment epithelium (RPE) is essential for healthy vision. Disrupted autophagy due to mTOR overactivation in the RPE is associated with blinding macular degenerations; however, outer segment degradation is unaffected in these diseases, indicating that distinct mechanisms regulate these clearance mechanisms. Here, using advanced imaging and mouse models, we identify optineurin as a key regulator that tunes phagocytosis and lysosomal capacity to meet circadian demands and helps prioritize outer segment clearance by the RPE in macular degenerations. High-resolution live-cell imaging implicates optineurin in scissioning outer segment tips prior to engulfment, analogous to microglial trogocytosis of neuronal processes. Optineurin is essential for recruiting LC3, which anchors outer segment phagosomes to microtubules and facilitates phagosome maturation and fusion with lysosomes. This dynamically activates transcription factor EB (TFEB) to induce lysosome biogenesis in an mTOR-independent, TRPML1 (transient receptor potential-mucolipin 1)-dependent manner. RNAseq analyses show that expression of TFEB target genes temporally tracks with optineurin recruitment, and that lysosomal and autophagy genes are controlled by distinct transcriptional

[*]**Correspondence to:** Aparna Lakkaraju (Aparna.Lakkaraju@ucsf.edu), Department of Ophthalmology, University of California, San Francisco, 10 Koret Way, K233, San Francisco, CA 94143. Phone: 415-502-9670, Twitter: @LakkarajuLab.

[4]Lead contact

Author Contributions

Conceptualization: A.L. and L.X.T.; data acquisition: L.X.T.; analysis of data: L.X.T.; resources: L.X.T., C.J.G., N.L., T.T.; writing of original draft: L.X.T.; writing, reviewing, and editing: L.X.T. and A.L.; project administration: A.L.

Declaration of interests

The authors declare no competing interests.

programs in the RPE. The unconventional plasma membrane-to-nucleus signaling mediated by optineurin ensures outer segment degradation under conditions of impaired autophagy in macular degeneration models. Independent regulation of these critical clearance mechanisms would help safeguard metabolic fitness of the RPE through the organismal lifespan.

Blurb

How phagocytic tissues balance phagolysosomal clearance and autophagy is unclear. Tan *et al.* identify a cell surface-to-nucleus signaling pathway regulated by optineurin that directs efficient circadian removal of phagocytosed photoreceptor outer segments by the retinal pigment epithelium, even under impaired autophagy, as in macular degenerations.

Graphical Abstract

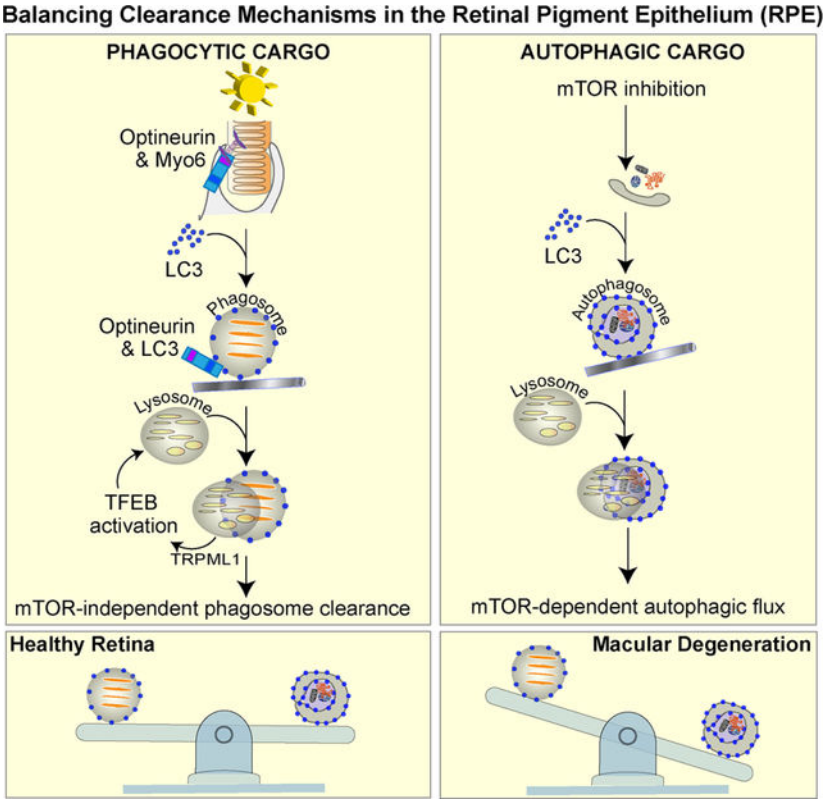

Keywords

phagocytosis; trogocytosis; TFEB; TRPML1; lysosomes; retinal pigment epithelium; photoreceptors; macular degeneration

Introduction

The recognition, engulfment, and degradation of pathogens and foreign material by phagocytosis is essential for tissue homeostasis. In the eye, phagocytosis and clearance of photoreceptor outer segments by the neighboring retinal pigment epithelium (RPE) is

a critical requirement for maintaining photoreceptor health and vision. Each day, the RPE phagocytoses and degrades 10% of distal photoreceptor outer segment discs as new discs are inserted at the base. This ensures removal of discs exposed to light damage as a consequence of phototransduction and helps recycle retinoids and fatty acid metabolites to the photoreceptors to support the visual cycle and photoreceptor metabolism [1,2].

Phagocytosis by the RPE is distinct from that performed by macrophages in that it is regulated in a circadian manner, and instead of the entire target cell, the RPE ingests and degrades only the damaged distal tips of photoreceptors, a process akin to trogocytosis or pruning of neurons by microglia [3,4]. The initial stages of outer segment recognition by the RPE are well characterized, from engagement of the αvβ5 integrin to activation of the Mer tyrosine kinase (MerTK) by soluble Gas6 and protein S, which bind phosphatidylserine on outer segment tips [5–7]. In contrast, the machinery that executes the final steps of trogocytosis i.e., scission of outer segment tips, is not well understood.

Another unresolved question is how the highly metabolically active postmitotic RPE scales lysosome capacity to meet daily degradative demands. In the human eye, each RPE cell ingests outer segment tips from ~40 photoreceptors every day, which constitutes an enormous burden on RPE lysosomes. In addition, the RPE needs to balance clearance of phagocytosed outer segments with removal of cellular debris by autophagy. Declining expression of autophagy machinery and inefficient autophagy in the RPE are implicated in the pathogenesis of inherited and age-related macular degenerations (AMD), which destroy central high-resolution vision in millions of people worldwide [8–10]. However, ingested outer segments appear to be degraded efficiently even under conditions of impaired autophagic flux [11,12], suggesting that the RPE prioritizes removal of phagocytosed cargo over intracellular debris. Here, using high-resolution and high-speed live imaging of the RPE from mice and cell-based models, we address how this prioritization is achieved and how the RPE dynamically tunes its degradative capacity to cope with circadian outer segment clearance.

Our studies identify three essential hierarchical functions for the autophagy receptor optineurin in regulating phagocytosis and lysosome biogenesis in the RPE: first, at the RPE plasma membrane optineurin participates in outer segment scissioning prior to ingestion; second, within the RPE, optineurin recruits LC3 to nascent phagosomes to facilitate their association with microtubules and subsequent fusion with lysosomes; and third, phagosome-lysosome interactions activate the lysosome calcium channel TRPML1 (transient receptor potential-mucolipin 1) to enable mechanistic target of rapamycin (mTOR)-independent nuclear translocation of the transcription factor EB (TFEB), which regulates lysosome gene expression. Association of optineurin with outer segment phagosomes at the plasma membrane parallels the circadian rhythm of TFEB activation, suggesting that this mechanism helps the RPE scale lysosome function to meet the daily demands of outer segment clearance. We further demonstrate that these noncanonical functions of optineurin are preserved in a mouse model of inherited macular degeneration with abnormal mTOR activation and defective autophagy in the RPE. Our studies identify key machinery and mechanisms that help the RPE prioritize outer segment clearance to safeguard photoreceptor health and vision.

Results

Scissioning of photoreceptor outer segments is facilitated by optineurin at the RPE cell surface.

To identify trogocytosis machinery in the RPE, we focused on proteins that interact with ubiquitinated cargo since photoreceptor outer segments are ubiquitinated [13]. We first investigated optineurin, a ubiquitin-binding adaptor protein that participates in multiple cellular processes including autophagy. During autophagy, ubiquitin binding to cytosolic optineurin via its UBAN (ubiquitin-binding domain of ABIN proteins and NEMO) domain could promote its interaction with the actin motor myosin VI (MYO6), which helps recruit it to nascent autophagosome membranes [14]. This tripartite adaptor/motor/membrane complex is known to facilitate autophagosome maturation. Based on these studies and others showing that optineurin and MYO6 cooperate to induce fission of melanosome tubules [15], we asked if optineurin functions in scissioning outer segments (Figure 1A). High-resolution immunofluorescence imaging of primary porcine RPE monolayers fed purified porcine rod outer segments (~40 outer segments/cell for 30 min at 37˚C) showed optineurin on rhodopsin-containing phagosomes (Figure 1B). In some cells, optineurin-positive structures extended outwards from the apical microvilli to interact with extracellular outer segments that were in the process of being internalized (Figures 1C, S1A, and S1B), indicating a role for optineurin at the plasma membrane *prior to* outer segment internalization. To determine whether optineurin facilitates outer segment trogocytosis, we performed high-resolution high-speed live-cell imaging of interactions between RPE expressing optineurin-GFP and Alexa647-labeled outer segments and captured optineurin in the process of actively scissioning outer segments (Figure 1D and Video S1). Analysis of ~1,200 phagosomes in ~300 RPE cells by immunostaining showed that optineurin was found on ~40% of outer segment phagosomes after 30 minutes, in agreement with our live imaging data (Figure 1E).

Quantification of optineurin association with outer segment phagosomes in mouse RPE flatmounts confirmed that this unconventional role of optineurin is conserved *in vivo*. Rod outer segment phagocytosis by the RPE follows a circadian rhythm, with peak phagocytosis occurring ~ 1 hour after light onset [16]. We observed optineurin localized to putative scission sites on outer segments at 1 h post-light onset (Figures 1F and 1G). 3D-reconstructions of outer segment phagosomes, optineurin, and actin at the apical surface of the RPE showed that optineurin is recruited early in the process, prior to sealing of the phagocytic cup (Figures 1H and 1I).

Immunofluorescence imaging of mouse RPE flatmounts showed that the actin motor MYO6 was present on ~90% of optineurin-positive phagosomes in 1 h after light onset (Figures 2A and 2B; also see Figures S1C and S1D). This suggests that at the apical surface of the RPE, optineurin likely regulates the activity of MYO6 to generate the mechanical force required for constricting outer segment tips prior to engulfment. To establish the role of the optineurin-MYO6 interaction in mediating outer segment internalization, we took advantage of an amyotrophic lateral sclerosis (ALS)-associated optineurin mutation, E478G, which abrogates the ability of optineurin to bind MYO6 [17,18]. We chose to use well-characterized mutant constructs to interrogate the role of specific optineurin binding

partners in the RPE, rather than knocking down optineurin using shRNA, which would not be as informative. Moreover, shRNA-mediated optineurin depletion caused widespread cell death in our primary RPE cultures. We expressed GFP-tagged wild type (WT) optineurin or the E478G mutant in the RPE and confirmed that both constructs were expressed at comparable levels, and equivalent to or higher than that of endogenous optineurin in the RPE (Figures S1E and S1F). Moreover, immunostaining of RPE cells after outer segment feeding showed that the E478G mutant is defective in recruiting MYO6 to outer segment phagosomes (Figures S1G and S1H).

Because E478G optineurin does not bind MYO6, we first examined its impact on outer segment scissioning. We performed live-cell imaging of primary RPE expressing either WT or E478G optineurin and fed Alexa647-labeled outer segments (Videos S1 and S2). Quantification of outer segment dynamics showed significantly fewer scission events occurring in RPE expressing E478G optineurin (Figure 2C).

To determine how loss of MYO6 recruitment affects phagocytosis, RPE monolayers were fed outer segments for 30 min, fixed, and immunostained for rhodopsin. To distinguish outer segments bound to the surface from those internalized in cells expressing WT or mutant optineurin, we immunostained for rhodopsin before and after permeabilization [19]. RPE expressing the E478G mutant optineurin ingested significantly fewer outer segments compared to cells expressing WT optineurin (Figures 2D, 2E, 2F, and S1I). This was not due to a mislocalization of the mutant protein as there was no difference in the apical distribution of WT and E478G (Figure 2G). Rather, RPE expressing E478G had significantly fewer optineurin-positive outer segment phagosomes compared to RPE expressing WT optineurin (Figure 2H). This suggests that the defect in OS scissioning could presumably impact both binding and internalization. To further investigate the involvement of MYO6 in outer segment phagocytosis, we treated primary RPE cells for 30 or 60 min with the MYO6 inhibitor 2,4,6-triiodophenol (TIP) [15,20,21] before outer segment feeding. Treatment with TIP for 60 min significantly reduced outer segment uptake by the RPE (Figures 2I and 2J). Collectively, these data suggest that optineurin and MYO6 act in concert to execute scissioning, binding, and ingestion of photoreceptor outer segment tips by the RPE. The importance of this interaction is illustrated by studies showing that loss of MYO6 inhibits phagosome clearance *in vitro* [22] and causes photoreceptor degeneration *in vivo* [23].

Oligomerization status of optineurin determines preferential association with outer segment phagosomes.

Optineurin was first identified as a mitophagy receptor [24], and in outer segment-fed primary RPE monolayers, we observed optineurin in association with both mitochondria and outer segment phagosomes (Figures 3A and 3B). Outer segment phagocytosis did not induce a change in the subcellular localization of optineurin (Figure 3C) or its association with mitochondria (Figure 3D). The amount of total cellular optineurin in association with outer segment phagosomes after 30 minutes was significantly lower than that in association with mitochondria (Figure 3E), likely reflecting the relative abundance of these organelles and the transient nature of optineurin association with mitochondria [25] or with phagosomes.

We next investigated mechanisms that could specify optineurin recruitment to phagosomes or mitochondria in the RPE. Based on reports that optineurin forms hexamers under oxidative stress [26], we asked whether optineurin oligomerization could dictate preferential association with either organelle. Primary RPE monolayers were either fed outer segments or treated with Urolithin A (UA, 100 μM, 24 h), which induces mitophagy [27], as a positive control. UA treatment induced the formation of ~420 kD optineurin oligomers, which are likely hexamers based on the predicted ~70 kD monomer size [26] as seen by native PAGE; in contrast, optineurin hexamers were not detected in naïve RPE monolayers or those fed outer segments (Figures 3F and 3G). Optineurin oligomers were also not observed in cells acutely treated with mitoChlorodinitrobenzoic acid (mitoCDNB, 5 μM, 30 min), which causes mitochondrial fragmentation by selectively depleting mitochondrial glutathione [28] but is not expected to induce mitophagy.

To confirm that monomeric optineurin associates with outer segment phagosomes, we performed a proximity ligation assay (PLA), which identifies protein-protein interactions within ~40 nm distance [26,29]. RPE cells expressing both GFP- and Flag-tagged optineurin were fed outer segments or treated with UA as above, and the number of PLA puncta/μm^3 in each condition was quantified (Figures 3H, 3I, S2A, and S2B). Consistent with our native PAGE data, mitophagy induction by UA significantly increased the number of PLA puncta on mitochondria, whereas outer segment phagosomes had very few PLA puncta. These data indicate that whereas optineurin oligomers dictate recruitment to mitochondria, optineurin monomers associate with outer segment phagosomes.

Optineurin recruits LC3 to nascent outer segment-containing phagosomes in the RPE.

What could be the physiological function of optineurin on outer segment phagosomes? Optineurin acts as an autophagy receptor by binding ubiquitinated cargo via its ubiquitin-binding domain and the autophagosome protein LC3 (microtubule-associated protein light chain 3) via its LC3 interacting region (LIR) domain [24]. LC3 also participates in the ingestion of pathogens, a process termed LC3-associated phagocytosis (LAP) that is distinct from canonical autophagy [30]. Although LC3 has been shown to associate with outer segment phagosomes [31,32] and deletion of LC3 leads to an accumulation of undegraded phagosomes in the RPE [33], mechanisms that regulate LC3 recruitment and how it functions in outer segment phagosome clearance are not well understood. Based on our live imaging data showing early association of optineurin with outer segments prior to the formation of nascent phagosomes, we reasoned that optineurin could recruit LC3 to phagosomes via its LIR domain [25].

Since outer segment phagocytosis is a circadian process that is modulated by light [16], we investigated the spatiotemporal dynamics of optineurin and LC3 association with outer segment phagosomes in mouse RPE flatmounts harvested at −1, 0, 1, and 3 h after light onset. High-resolution immunofluorescence imaging and quantification of ~2,400 phagosomes in mouse RPE per time point revealed that maximal optineurin recruitment to phagosomes coincides with the time of peak outer segment phagocytosis, at 1 h post-light onset, whereas maximal LC3 recruitment occurs at 3 h post-light onset (Figures 4A, 4B, S3A, and S3B). As further proof that optineurin is recruited early in the phagocytic

process and precedes LC3 recruitment *in vivo*, we quantified optineurin association with phagosomes labeled with an antibody that recognizes the C-terminus of rhodopsin in mouse RPE flatmounts at 1 h after light onset (Figures S3C and S3D). As the C-terminus is degraded soon after phagocytosis, phagosomes labeled with this antibody are termed "early" phagosomes [34]. To confirm this hierarchical recruitment of optineurin and LC3 to outer segment phagosomes, we performed a synchronized phagocytosis assay by feeding polarized primary RPE monolayers with ~40 outer segments/cell for 30 min, after which unbound outer segments were removed and the cells incubated in fresh medium for defined time periods ("chase"). In agreement with our *in vivo* data, optineurin association with outer segments preceded LC3 recruitment (Figures 4C, 4D, S3E, and S3F).

LC3 is a cytosolic protein that is covalently bound to phosphatidylethanolamine (lipidated) by the ATG12–5-16L1 complex on phagosomal membranes [30]. Recruitment of this complex depends on the generation of phosphatidylinositol-3-phosphate (PI3P), which activates WIPIs (WD-repeat PI3P effector proteins) to directly recruit the ATG16L1 complex [35]. Atg16L1 also binds optineurin [36], suggesting that optineurin recruits both LC3 and its lipidation machinery to outer segment phagosomes. Analysis of immunostained mouse RPE flatmounts at 3 h after light onset revealed the presence of both Atg16L1 and early endosomal autoantigen 1 (EEA1), which marks regions of high membrane PI3P, on outer segment phagosomes (Figure S3G).

To establish the importance of optineurin-LC3 interaction in outer segment phagocytosis, we expressed GFP-tagged constructs of either WT optineurin or the F178A mutant, which has a point mutation in the LIR that abrogates binding to LC3 [25,37,38], in primary RPE monolayers (Figures S3H and S3I). Quantification of outer segment uptake after synchronized phagocytosis showed that RPE expressing F178A mutant optineurin had significantly fewer LC3-positive phagosomes compared to RPE expressing WT optineurin (~24% LC3+ phagosomes in WT RPE vs ~6% in F178A RPE) (Figures 4E and 4F). Although there was no difference in the apical localization of F178A mutant compared to WT optineurin (Figure 4G), F178A optineurin had significantly reduced association with LC3, as reported by others [25,37] (Figure 4H).

RPE expressing F178A showed reduced outer segment phagocytosis, though to a significantly lesser extent than the E478G mutant (Figures 4I and 4J). The F178A mutation is located within the region required for interaction with the small GTPase RAB8 (Ras-related protein Rab8) [39], which has been shown to mediate phagocytosis in macrophages and microglia [40]. To investigate if the F178A mutation disrupts optineurin-RAB8 binding and if RAB8 participates in outer segment phagocytosis, we quantified co-localization of wild-type and F178A optineurin with RAB8 in primary RPE fed outer segments. Our data show that the F178A mutation does not alter the association of RAB8 with either optineurin (Figures 4K and 4L) or outer segments (Figure 4M). This suggests that the decreased outer segment uptake in cells expressing F178A optineurin is likely due to a failure in amplifying optineurin recruitment. LC3 recruited by optineurin has been shown to initiate a feed-forward loop to recruit more optineurin to the membrane [38]. In the context of outer segment phagocytosis, loss of LC3-optineurin association in cells with F178A (Figure 4H) would prevent further optineurin recruitment to the phagosome, thereby resulting in

reduced outer segment uptake. This also explains why inhibition of outer segment uptake in F178A-expressing cells is milder compared to that of E478G-expressing RPE (Figures 4I and 4J). Taken together, these data demonstrate that optineurin is essential for recruiting LC3 to outer segment phagosomes in the RPE.

LC3 anchors phagosomes to microtubules and promotes phagosome-lysosome interactions.

Mice deficient in LAP exhibit delayed phagosome clearance and develop retinal deficits [31–33], suggesting that LC3 association is important for outer segment degradation and for maintaining visual function. But precisely how does LC3 modulate phagosome clearance in the RPE? Since LC3 was first isolated as a microtubule-associated protein [41], we asked if LC3 mediates association between phagosomes and microtubules. Quantification of phagosomes in mouse RPE flatmounts after immunostaining with tubulin and rhodopsin at 1 h post-light onset showed that a significantly higher percentage of LC3-positive outer segment phagosomes are anchored to microtubules compared to phagosomes without LC3 (Figures 5A, 5B, and 5C). Outer segment phagosomes are transported by microtubules from the apical side of the RPE towards the basolateral side [42]. If LC3 indeed connects phagosomes with microtubules, then LC3-associated phagosomes should be localized more towards the basal side of the RPE than phagosomes lacking LC3. Analysis of the relative location of LC3-positive and LC3-negative phagosomes as a function of cell height showed that phagosomes without LC3 are significantly more apical compared to those with LC3 (Figures 5D, 5E, and 5F), consistent with the role of LC3 in mediating microtubule-based, apical-to-basal trafficking of phagosomes.

Transport of phagosomes along microtubules facilitates phagosome-lysosome interactions to execute degradation of phagocytosed cargo [43]. Although LC3-association has been shown to promote phagolysosomal clearance of apoptotic cells by macrophages [44], it impedes removal of phagosomes sequestering bacterial pathogens [45], suggesting a cargo-dependent role of LC3 in phagosome maturation. To evaluate how LC3 impacts outer segment phagosome maturation, we monitored interactions between LC3, outer segments, and lysosomes in primary RPE monolayers using high-speed, high-resolution live-cell imaging. Cells transduced with BacMam LC3B-GFP were incubated with Lysotracker Red to label lysosomes and fed Alexa647-labeled outer segments. Quantification of live imaging data showed that lysosomes interact to a significantly greater extent with LC3-positive outer segment phagosomes compared with LC3-negative phagosomes (Figures 5G, 5H, and Video S3).

To better delineate the importance of LC3 in anchoring outer segments to microtubules, we quantified phagosome-microtubule and phagosome-lysosome interactions in RPE expressing either WT optineurin or the F178A mutant optineurin, which cannot recruit LC3. No obvious differences in either microtubule organization or lysosome numbers were observed between RPE expressing WT or F178A optineurin. However, association of outer segment phagosomes with microtubules (Figures 5I and 5K) and with lysosomes (Figures 5J and 5L) were significantly decreased in RPE expressing F178A optineurin. These data

demonstrate that optineurin and LC3 recruitment to outer segment phagosomes is essential for microtubule-based phagosome trafficking and maturation.

Outer segment phagocytosis induces TRPML1-mediated nuclear translocation of TFEB.

The spatiotemporal dynamics of optineurin and LC3 association with phagosomes prompted us to investigate whether this mechanism regulates scaling of lysosomal capacity to ensure efficient phagosome degradation in the RPE. To test this hypothesis, we focused on the transcription factor EB (TFEB), a master regulator of autophagy and lysosome genes. Upon activation by nutrient deprivation or other stressors, TFEB translocates from the cytoplasm to the nucleus, where it binds CLEAR (*c*oordinated *l*ysosomal *e*xpression *a*nd *r*egulation) motifs within the promoters of target genes, including optineurin, LC3, and LAMP1/2 (lysosome-associated membrane proteins 1 and 2) to drive their expression [46]. Analysis of GFP-TFEB localization by high-speed live-cell imaging of transiently transfected primary RPE monolayers showed that either serum starvation (a known TFEB activator [47]) or outer segment phagocytosis induce robust nuclear translocation of GFP-TFEB within ~50 min (30 min outer segment feeding + ~20 min live imaging) (Figures 6A and 6B, Videos S4, S5, and S6). Immunoblotting of cytoplasmic and nuclear fractions of primary RPE cells for endogenous TFEB after outer segment phagocytosis confirmed our live imaging data (Figures S4A and S4B).

If outer segment phagocytosis indeed triggers TFEB activation, then nuclear localization of TFEB should follow a circadian rhythm that parallels that of outer segment phagocytosis. Quantification of nuclear and cytoplasmic TFEB by immunostaining mouse RPE flatmounts with a knockout-validated TFEB antibody [48] showed peak TFEB activation at 0 and 5 h after light onset (Figures 6C and 6D). RNAseq analyses of mouse RPE showed that expression of several TFEB targets correlated with the TFEB activation peak at 5 h post-light onset (Figure 6E). The purity of mouse RPE isolation was confirmed by the negligible expression of choroidal genes in the RNAseq datasets (Figure S4C).

How would phagocytosis of outer segments at the plasma membrane induce translocation of TFEB into the nucleus? In resting cells, TFEB is sequestered in the cytoplasm upon phosphorylation by the kinase mTOR [49]. Either mTOR inhibition or TFEB dephosphorylation by the calcium-regulated phosphatase calcineurin results in nuclear transport of TFEB. The lysosomal calcium channel TRPML1 has been implicated in activating calcineurin to drive TFEB translocation independent of mTOR activation status [50,51]. Based on our previous studies showing that outer segment clearance proceeds normally in RPE with abnormally active mTOR [11], we hypothesized that TFEB activation in response to outer segment phagocytosis is likely regulated by TRPML1-mediated calcineurin activation. To test this, we first asked whether outer segment phagosomes interact with lysosomes within the 50 min (30 min feeding + 20 min imaging) that we observed TFEB nuclear translocation by live imaging (Figures 6A and 6B). Immunostaining of outer segment-fed primary RPE monolayers showed that ~29% of outer segment phagosomes associate with LAMP2-positive lysosomes within the 50 min window (Figures S4D and S4E). A short treatment with MLSI3 [52], a specific TRPML1 inhibitor, prevented TFEB

nuclear translocation in response to outer segment phagocytosis (Figures 6F and 6G), suggesting that TRPML1 is responsible for the diurnal TFEB activation in the RPE.

We next investigated whether interfering with optineurin and LC3 recruitment early in phagocytosis would impact TFEB nuclear translocation. Primary RPE expressing F178A mutant optineurin, which cannot bind LC3, had significantly less nuclear TFEB upon outer segment phagocytosis compared to cells expressing WT optineurin (Figures 6H and 6I). Thus far, our studies identify an outside-in signaling pathway where optineurin recruitment to outer segment phagosomes at the plasma membrane leads to TRPML1-dependent nuclear transport of TFEB.

TFEB activation in response to outer segment phagocytosis is maintained under conditions of impaired autophagy.

Our previous studies show that clearance of phagocytosed outer segments by the RPE proceeds efficiently in the *Abca4*$^{-/-}$ mouse model of Stargardt's inherited macular degeneration, despite abnormal mTOR activation, decreased autophagosome biogenesis, and accumulation of autophagic cargo in *Abca4*$^{-/-}$ RPE [11,12]. These data suggest that outer segment clearance is likely regulated independent of autophagy in the RPE. To better understand this, we compared optineurin and LC3 association with outer segments, phagosome-lysosome fusion, and TFEB nuclear translocation in WT and *Abca4*$^{-/-}$ mouse RPE flatmounts. Quantification of optineurin and LC3 recruitment to outer segments at the times of peak association (1 h and 3 h post-light onset, respectively) revealed no differences between WT and *Abca4*$^{-/-}$ RPE (Figures 7A–7C, and S5). Neither did we observe any deficits in phagosome maturation as quantified by colocalization between rhodopsin and lysosomal markers LAMP1 and LAMP2 (Figures 7D and E). Moreover, despite increased mTOR activation in *Abca4*$^{-/-}$ RPE [11], TFEB nuclear translocation at the 5 h post-light onset peak was comparable to that of WT mice (Figures 7F and 7G). Bulk RNAseq (Figures 7H and S6A) and qPCR (Figure S6B) analyses revealed comparable expression of TFEB target gene transcripts in WT and *Abca4*$^{-/-}$ mouse RPE.

Whereas TFEB regulates both autophagy and lysosomal genes, the Forkhead Box O3 (FOXO3) transcription factor predominantly regulates autophagy genes [53]. Like TFEB, FOXO3 also translocates to the nucleus upon activation to initiate the transcription of target genes. To determine whether outer segment phagocytosis specifically activates TFEB, we followed FOXO3 translocation by immunostaining naïve primary RPE monolayers or after outer segment phagocytosis. We observed no discernible change in FOXO3 nuclear localization in response to outer segments (Figures S6C and S6D). Further, shRNA-mediated knockdown of FOXO3 did not affect outer segment uptake or degradation (Figures S6E–S6G), suggesting that outer segment phagocytosis specifically activates TFEB. Collectively, these data demonstrate that outer segment phagocytosis specifically activates TFEB independent of mTOR, which likely helps the RPE preferentially clear phagocytosed outer segments under conditions of aberrant mTOR activation and impaired autophagy.

Discussion

Phagocytosis is a dynamic process regulated at the cell surface by receptor expression, cytoskeletal remodeling, and inside-out signaling [3]. Our data now identify optineurin as a previously unrecognized player in regulating the plasticity of photoreceptor outer segment phagocytosis and clearance by the RPE at multiple steps (Figure 7I). First, using quantitative live-cell imaging and high-resolution microscopy, we answer a long-standing question in the field and show that optineurin working in concert with the actin motor MYO6 participates in the trogocytosis of distal outer segment tips at the apical surface of the RPE. This temporally and spatially constrained association of optineurin with outer segments and outer segment phagosomes that we report is essential for maintaining the circadian rhythm of this process. The autophagy receptors TAX1BP1 (Tax1 binding protein 1) and NDP52/CALCOCO2 (nuclear dot protein 52 kDa/calcium binding and coiled-coil domain 2) also bind the C-terminal cargo-binding domain of MYO6 [54,55], but the functional relevance of these interactions is not clear. MYO6 has been implicated in initiating the formation of actin-rich cages that enwrap damaged mitochondria to prevent mitochondrial fusion, but this occurs independent of autophagy receptors [56]. This suggests that optineurin is unique in regulating MYO6-mediated fission of melanosome tubules reported previously [15] and outer segment tips observed here. Indeed, our data are consistent with a recent report implicating actin remodeling in outer segment trogocytosis by the RPE [4].

Second, we show that optineurin is essential for recruiting LC3 to outer segment phagosomes in the RPE, which in turn promotes phagosome-lysosome interactions by linking phagosomes to microtubules. These data help explain previous observations that inhibiting LC3 association disrupts phagosome clearance and interferes with recycling of products of phagolysosomal degradation to the photoreceptors [31–33].

Third, we identify a molecular mechanism to decipher the paradoxical observation of efficient phagosome clearance under conditions of significant autophagic defects in the RPE. We establish optineurin as a critical regulator of a novel outside-in signaling pathway that mediates mTOR-independent TFEB activation to help the RPE scale its degradative capacity to meet the immense demands of outer segment clearance. This helps the RPE safeguard outer segment degradation under conditions of aberrant mTOR activity (and thereby, impaired autophagy) seen in aging and diseased RPE [11,57–59]. Prioritizing outer segment clearance also ensures efficient recycling of retinoids to the photoreceptors required to maintain healthy vision [31–33]. The FOXO family of transcription factors, specifically FOXO3, regulates expression of autophagy genes but is not involved in, or activated by, outer segment phagocytosis in the RPE. Given that the RPE, which is the most active phagocyte in the body, is also a postmitotic highly metabolically active tissue, independent regulation of these critical clearance mechanisms would help safeguard metabolic fitness of the RPE.

Our studies have implications beyond the retina: in the brain, overactive mTOR, defective autophagy, and debris accumulation are features of dysfunctional microglia in aging and Alzheimer's disease models [60,61], and efficient LC3-associated phagocytosis by microglia helps degrade myelin and prevents progression of multiple sclerosis [62]. Whether optineurin

is involved in regulating microglial phagocytosis and TFEB activation are important and intriguing questions that remain to be answered, given the association of optineurin loss-of-function mutations with amyotrophic lateral sclerosis and other neurodegenerative diseases. This research provides important insight into how differential regulation of clearance mechanisms could maintain the metabolic fitness of postmitotic highly phagocytic cells and thereby exacerbate or mitigate neurodegenerative diseases.

STAR Methods

Resource availability

Lead contact

Further information and request for resources and reagents should be directed to and will be fulfilled by the lead contact, Aparna Lakkaraju (Aparna.Lakkaraju@ucsf.edu)

Materials availability

This study did not generate new unique reagents.

Data and code availability

- Bulk RNA-seq data have been deposited at GEO and are publicly available as of the date of publication. Accession numbers are listed in the key resources table. Original western blot images have been deposited at Mendeley and are publicly available as of the date of publication. The DOI is listed in the key resources table. Microscopy data reported in this paper will be shared by the lead contact upon request.
- This research has not generated any original code.
- Any additional information required to reanalyze the data reported in this paper is available from the lead contact upon request.

Experimental models and details

Mice.—All animal experiments were approved by the Institutional Animal Care and Use committees at the University of Wisconsin–Madison and the University of California, San Francisco. Wild-type (Jackson Labs; 129S1/SvlmJ) and *Abca4*$^{-/-}$ mice (Jackson Labs *Abca4tm1Ght/J*), both on Rpe65 Leu450 background were raised under 12-h cyclic light with standard diet. Mice were sacrificed at the indicated times after light onset, eyes were removed, and eyecups were processed for immunohistochemistry, transcriptomics, or biochemical studies as detailed below. GFP-LC3 mice were obtained from the Debnath Lab at the University of California, San Francisco. Equal number of ~6-month-old male and female mice were used for the analyses.

Primary porcine RPE cell cultures.—Primary RPE were isolated from porcine eyes using established protocols [69]. To generate polarized cultures, cells were plated at ~350,000 cells/cm^2 onto collagen-coated Transwell filters (Corning, Corning, NY). These RPE form fully polarized monolayers within two weeks with trans-epithelial electrical resistances

(TER) of ≥ 400 ohm.cm^2 and express RPE differentiation markers such as apical Na^+,K^+-ATPase and intracellular RPE65.

Method details

Porcine rod photoreceptor outer segment isolation.

Rod outer segments were isolated from freshly harvested retinas according to established protocols [70]. Briefly, retinas were dissected from pig eyes under dim light and homogenized. After removing large aggregates by filtration, homogenates were loaded onto 60%–25% sucrose gradients. After ultracentrifugation at 26,000 rpm for 1 h at 4°C, the pink band near the upper-third of the gradient containing outer segments was collected. Isolated outer segments were washed (three times at 3,000×*g*, 4°C), resuspended in DMEM with 2.5% sucrose and stored at −80°C in single-use aliquots.

Outer segment phagocytosis assays and inhibitors.

Polarized primary adult porcine RPE monolayers were fed purified porcine outer segments at ~40 outer segments/cell for 30 min at 37°C [69]. Cells were rinsed 3 times with 1X PBS to remove unbound outer segments and re-incubated in 1% FBS media for the indicated chase periods. For live-cell imaging (see below), outer segments were labeled with 0.035 mg/ml TRITC (ThermoFisher Scientific, Waltham, MA; T490) or 0.06 mg/ml Alexa Fluor 647 NHS Ester (ThermoFisher Scientific, Waltham, MA; A20006) with rotation for 1 h at room temperature in the dark and rinsed three times in 1X PBS prior to adding to the cells. To inhibit MYO6, RPE were pre-treated with 40 μM 2,4,6-triiodophenol (TIP) for 30 or 60 min before addition of outer segments in the presence of TIP. Cells fed outer segments without TIP treatment were used as controls. After removal of unbound outer segments, cells were harvested and processed for immunoblotting (see below).

For immunostaining of outer segments, the mouse anti-rhodopsin (4D2) antibody which recognizes the N-terminus, was used unless otherwise stated. To distinguish outer segments bound to the cell surface from those internalized by the RPE, cells were first stained with the 4D2 rhodopsin antibody without permeabilization (no saponin), followed by staining with AlexaFluor anti-mouse 647. After three 5 min rinses in 1% BSA/PBS and one 5 min rinse in 1X PBS, cells were fixed in 2% paraformaldehyde for 5 min at room temperature. Cells were then stained again with 4D2 in the presence of 0.1% saponin, followed by incubation with AlexaFluor anti-mouse 568 secondary antibody. Internalized outer segments are only labeled with AlexaFluor 568, while outer segments bound to the surface are labeled with both secondary antibodies [19].

Cloning of optineurin mutant plasmids.

pBMN mEGFP-OPTN(F178A) (Addgene #119681) was restriction digested from the respective plasmids with BamHI-HF (New England BioLabs, R3136T) and XhoI (New England BioLabs, R0146S) and ligated into pEGFP-C1 plasmids (Clontech) digested with the same enzymes.

Transfection of polarized primary RPE monolayers.

Primary RPE were transfected with the indicated plasmids at 5–10 μg for ~1.5×10^6 cells using Amaxa nucleofector II (Lonza, Rockland, ME) [71] or magnetofected with 0.5 μg plasmid/~3×10^5 cells using LipoMag Transfection Kit (OZ Biosciences, San Diego, CA).

High-resolution high-speed live-cell Imaging.

Primary RPE monolayers expressing pOPTN-EGFP, LC3B-GFP (BacMam), or TFEB-GFP were fed fluorescently labeled (TRITC or Alexa647-NHS ester, as detailed above) purified porcine outer segments at ~40 outer segments/cell for 30 min at 37°C. Unbound and uninternalized outer segments were removed by rinsing in 1X PBS. Where indicated, cells were labeled with Lysotracker Red (Invitrogen) at 200 nM for 15 min at 37°C, or with CellMask Orange (Invitrogen) at 2.5 μg/mL for 5 min at 37°C prior to imaging. Cells were imaged in recording media (1X HBSS, 4.5 g/L glucose, 0.01 M HEPES) supplemented with 1% FBS and 1% NEAA as described previously [8,12,72,73]. Imaging was performed at 37°C in an Okolab humidified microenvironmental chamber on the Nikon spinning disk confocal microscope using a CFI60 Apochromat TIRF 100X oil immersion objective (1.49 NA). The system is equipped with: Yokogawa CSU-X1 confocal spinning disk head, Nikon Eclipse Ti2-E inverted microscope, Live-SR super-resolution module, Andor iXon Ultra 888 EMCCD camera, TI2-S-SE-E motorized stage with piezo-Z for rapid Z-stack acquisition, and a laser combiner with four solid-state lasers at 405, 488, 561, and 640 nm and the corresponding band-pass emission filter sets (Chroma) loaded on a FLI high speed filter wheel. The Live-SR is a super-resolution module that increases x-y resolution to ~ 120–140 nm, making it comparable to the resolution achieved by structured illumination microscopy (SIM). Identical laser power, exposure and gain settings were applied for all conditions within a set of experiments. Intervals and durations for timelapse acquisitions were: OPTN-EGFP (both WT and E478G) (30 sec intervals for 15 min), LC3B-GFP (1 min intervals for 10 min), TFEB-GFP (30 sec intervals for 20 min). Interactions between optineurin and LC3B with outer segments were quantified using object-based colocalization in Imaris (see below).

Immunofluorescence staining of primary RPE cultures.

RPE monolayers on Transwell filters were fixed with 2% paraformaldehyde for 10 min and blocked in 1% bovine serum albumin (BSA) in phosphate-buffered saline (PBS) for 30 min. For TFEB staining, cells were permeabilized with 0.1% Triton-X in 1% BSA for 30 min at room temperature to enable nuclear penetration of the antibody. Cells were then stained with the specific antibodies diluted in 1% BSA supplemented with 0.1% saponin for 1 h at room temperature (see Table S1 for antibody sources and dilutions). After three 5 min rinses, cells were stained with AlexaFluor secondary antibodies (ThermoFisher Scientific, Waltham, MA) at 1:500 and rhodamine–phalloidin (Cytoskeleton, Denver, CO; PHDR1) at 1:200 in 1% BSA for 30 min at room temperature. Nuclei were stained with DAPI at 1:200 (Sigma-Aldrich, St. Louis, MO; D9542) for 5 min followed by three 5 rinses. Filters were mounted and sealed under coverslips on glass slides with Vectashield (Vector Labs, Peterborough, UK).

Immunostaining of mouse RPE flatmounts.

Mouse eyes were collected at the indicated times after light onset. Anterior portions of the eyes including the lens were removed. Four relaxing cuts were made on the remaining eye cups, which was then fixed in 4% PFA for 2 h at room temperature. After three 5 min rinses with PBS, the retinas were clipped and removed, and relaxing cuts were made. Each RPE flatmount was then blocked for 1 h at room temperature in 300 μL of 2% BSA in PBS supplemented with 0.1% Triton-X. Flatmounts were incubated with indicated primary antibodies (see Table S1) diluted in 1% BSA in PBS at 4°C overnight. Flatmounts were rinsed in PBS, three times for 10 min each, with gentle shaking, and incubated for 2 h at room temperature in AlexaFluor secondary antibodies (1:500, ThermoFisher Scientific, Waltham, MA), diluted in 1% BSA. After secondary staining, flatmounts were rinsed as above and stained with DAPI (Sigma-Aldrich, St. Louis, MO; D9542, 1:200 in PBS for 15 min at room temperature). After three rinses, RPE flatmounts were mounted and sealed on clean slides with PBS and Vectashield (Vector Labs, Peterborough, UK).

Image analysis.

Images were captured on the spinning disk confocal microscope using 100×/1.49 NA oil objective. The same laser power and exposure time was used for each antibody within a set of experiments. Images were subjected to Gaussian filtering, background subtraction, and object-based colocalization analyses in Imaris. Where indicated, the image was subjected to automatic 3D deconvolution using NIS-Elements (Nikon, Tokyo, Japan). Intensity profiles were generated by drawing a line along the indicated axes in NIS-Elements (Nikon). Intensity values were then exported and compiled in Microsoft Excel and plotted using Prism 8 (GraphPad). Insets for line intensity profiles were exported from NIS Elements using the “Create View Snapshot” function. To quantify interaction between outer segment phagosomes, OPTN, LC3B, LAMP1, LAMP2, MYO6, RAB8, tubulin, or MYO6, surface rendering was performed using the “Surfaces” or “Spots” module in Imaris (Bitplane). Object-based colocalization was then performed using the “shortest distance” filter to quantify touching objects.

Analysis of outer segment scissioning.—Timelapse movies were subjected to surface tracking in Imaris using the “Connected Components” algorithm. Detected scission events were confirmed manually by scrolling through the timelapse movies. The number of track split was obtained from the statistics tab and compiled in Microsoft Excel as number of scission events.

Analysis of phagosome z-position.—Surfaces were created for outer segment phagosomes using the “Surfaces” tool in Imaris, with the same threshold values applied for all images. LC3-positive phagosomes were selected using intensity threshold, and the selected surfaces were duplicated into a new surface. The remaining phagosomes were defined as LC3-negative. The z position for each phagosome was exported from the statistics tab (separately for LC3-positive and LC3-negative phagosomes) and compiled in Microsoft Excel. For each field, the top and bottom z-values were obtained from image metadata and used for normalization of phagosome z-positions as a function of cell height in Microsoft Excel. Compiled data were plotted using Prism (GraphPad).

Analysis of apical-basal localization of wildtype and mutant optineurin.—Spots were created for OPTN-GFP (WT, F178A, and E478G) with the "Spots" tool in Imaris using the same quality threshold values for all conditions. The z position for each spot was exported from the statistics tab and compiled in Microsoft Excel. The top (apical) and bottom (basal) z positions of the cells were obtained from image metadata and used to calculate the position of each OPTN spot relative to the corresponding cell height (z position of spot minus bottom position of the cell, divided by the height of the cell). The percentage of puncta within the top 20% of cell height were then computed, and statistical analysis performed in Prism (GraphPad).

Quantification of nuclear and cytoplasmic ratios of TFEB and FOXO3.—To quantify nuclear and cytoplasmic TFEB and FOXO3, surface reconstructions of the DAPI channel were first created using the "Surface" tool in Imaris. Nuclear TFEB and FOXO3 signal intensities were exported from the statistics tab under the created surface. For cytoplasmic signal, a mask was created using the nuclei surface by setting any signal within the surface to 0. TFEB and FOXO3 signals of the mask channel were exported from the statistics tab and compiled in Microsoft Excel. Mean intensities generated from Imaris were normalized to the number of voxels, which correlates with the surface volumes.

Proximity ligation assay.

Primary porcine RPE were transfected with pOPTN-EGFP (Addgene) and Flag-OPTN (SinoBiological) and treated as indicated depending on the experimental design. Cells were fixed with 2% PFA for 10 min and permeabilized with 0.1% Triton-X for 10 min at room temperature. The proximity ligation assay was performed using Duolink® Proximity Ligation Assay (Millipore) according to manufacturer's protocol. Cells were immunostained with antibodies to Flag (Cell Signaling) and CF®405M-conjugated TOM20 (Santa Cruz) or DyLight™ 405-conjugated Rhodopsin (Millipore) antibodies. The number of PLA puncta were quantified in Imaris (Bitplane). Mitochondria and outer segment phagosomes were subjected to surface rendering using the "Surfaces" module, and the corresponding volumes were exported from the statistics tab in Imaris (Bitplane). Data were compiled in Microsoft Excel and plotted in Prism (GraphPad).

Immunoblotting.

For **NativePAGE**, trypsinized primary porcine RPE monolayers were processed using the NativePAGE sample prep kit (Invitrogen, BN2008). Lysates were resolved in NativePAGE 4–16% Bis-Tris gel (Invitrogen BN1004BOX) and transferred onto PVDF membranes (iBlot, Thermo Fisher). Optineurin oligomers were detected by probing the membrane with rabbit anti-optineurin antibody (Genetex, 1:1000 for 16 h at 4°C), followed by LiCOR IRDye and imaged on the LI-COR Odyssey CLx scanner. For **SDS-PAGE,** Cells were lysed in RIPA buffer (Abcam) supplemented with protease inhibitor cocktail and 1 mM PMSF (Tocris). Protein concentrations were measured by DC Protein Assay (Bio-Rad). Laemmli SDS-Sample Buffer (BioWorld) were added to ~40 μg lysates and samples were heated at 95°C for 5 min. Samples were resolved in NuPAGE 4–12% Bis-Tris gel (Invitrogen) at 150V for ~1 h at room temperature. Gels were transferred onto nitrocellulose membranes

using the iBlot transfer device (Invitrogen) for 7 min using the preset program 3. Blocking, immunoblotting, signal detection and analyses were performed as detailed above.

Nuclear/Cytoplasmic fractionation.

Nuclear and cytoplasmic fractions were harvested from pig RPE cells using NE-PER Nuclear and Cytoplasmic Extraction Reagents (ThermoFisher, 78833) according to manufacturer's protocol: Control and outer segment-fed RPE were harvested via trypsinization and cell pellets were washed once with 1X PBS. Cell pellets were then resuspended in ice-cold CER I supplemented with protease inhibitor cocktail via vigorous vortexing at the highest setting for 15 s and incubated on ice for 10 min. Ice-cold CER II was added to the cell suspension, followed by vigorous vortexing for 5 s at the highest setting. Cell suspension was incubated on ice for 1 min, vortexed for 5 s, and centrifuged at maximum speed for 5 min at 4°C. Cytoplasmic fractions were collected into a pre-chilled microtube and kept on ice until use. The remaining pellet was resuspended in ice-cold NER, vortexed for 15 s, and incubated on ice for 10 min. Vortexing and incubation were repeated every 10 min for a total of 40 min. Samples were centrifuged at maximum speed for 10 min at 4°C, and nuclear fractions were carefully collected into a pre-chilled microtube and kept on ice. Both fractions were subjected to DC protein assay (Bio-Rad) to measure protein concentrations. Lysates (~20 μg) were prepared for SDS-PAGE by adding 4X NuPAGE LDS sample buffer and 10x reducing agent (both used at 1x final concentration) (Invitrogen), followed by heating at 70°C for 10 min. Samples were then resolved in 4–12% bis-tris gels (Invitrogen) at 150V for ~1 h at room temperature. Gel was transferred onto nitrocellulose membrane and immunoblotting was performed as detailed above.

***Foxo3* knockdown.—**Primary RPE were transfected with scrambled shRNA or *Foxo3* shRNA (Origene) (~5 μg plasmid for 1.5×10^6 cells) and seeded onto 12-well plates. See Table S1 for shRNA sequence. Significant knockdown of FOXO3 (~30% of scrambled) was observed at 5 days post-transfection. Scrambled or *Foxo3* shRNA expressing RPE were fed ~40 outer segments/cell for 30 min followed by 0 or 5 h chase period. Cells were harvested via trypsinization, lysed in 1X HNTG lysis buffer (50 mM HEPES, 150 mM NaCl, 10% glycerol, 1.5 mM MgCl2, 1% Triton X-100) supplemented with protease inhibitor cocktail, and processed for immunoblotting as above.

RNA sequencing and analysis.

Mice were sacrificed at the indicated times after light onset and enucleated eyes were processed as detailed above. Eyecups were the placed in a pre-chilled RNase-free microcentrifuge tube and kept on ice at all times. Disposable plastic pestles were used to dissociate RPE from the eyecups into sterile 1X PBS, with gentle twisting motion applied to the RPE side. RPE suspension for both eyes from the same mouse were pooled and lysis buffer provided in the RNAqueous™-Micro Total RNA Isolation Kit (Thermo Fisher, AM1931) was added immediately. Total RNA was isolated according to manufacturer's protocol. Cell lysates were vortexed at maximum speed for 20 seconds. Half-volume of molecular-grade ethanol was added followed by brief vortexing. Lysates were passed through the Micro filter cartridge with 14,000×*g* centrifugation, followed by 3 washes using the wash solutions provided in the kit. Finally, the RNA was eluted in the elution

buffer provided and subjected to DNase I treatment. Samples were submitted to Novogene (Sacramento, CA) for bulk RNA sequencing using Illumina NovaSeq6000 platform. All samples were confirmed to have RIN > 7 prior to sequencing assessed using the RNA Nano 6000 Kit of the Bioanalyzer 2100 system (Agilent Technologies, CA). FASTQ were processed through fastp, and paired-end clean reads were aligned to the reference genome using the Spliced Transcripts Alignment to a Reference (STAR) software. FPKM of selected genes were compiled in Microsoft Excel and normalized to the expression at light onset. For statistical analyses, each timepoint was subjected to pair-wise comparisons with that at light onset using DESeq2 [74] in R-studio. Heatmaps were generated using the heatmap.2 function within gplots (https://CRAN.R-project.org/package=gplots).

qPCR.

RNA was isolated from mouse eyecups using RNAqueous™-Micro Total RNA Isolation Kit (Thermo Fisher, AM1931) and treated with DNase I as described above for RNA sequencing. Reverse transcription of RNA was performed using the iScript cDNA synthesis kit (1708890, Bio-Rad), and qPCR reactions were performed with CFX96 Thermal Cycler Real Time System (Bio-Rad). 18s was used as house-keeping gene. ΔΔCq was calculated as ((Cqtarget − Cq18s) − (WT1 Cq_{target} − WT1 Cq_{18s}). Relative expression was calculated by normalizing $2^{-\Delta\Delta Cq}$ to mean WT values. Primers for qPCR were purchased from Integrated DNA Technologies (IDT). Specificity of the primers were confirmed by presence of a single peak in the melt curves.

Quantification and Statistical Analysis.

Statistical analyses were performed using Prism 9 (GraphPad). Details of all statistical tests, sample sizes, and statistical significance are reported in the figure legends. Unless otherwise noted in the legend, data are presented as means and error bars represent SEM. Statistical significance was defined as p-value < 0.05.

Supplementary Material

Refer to Web version on PubMed Central for supplementary material.

Acknowledgments

Supported by NIH grants R01EY023299 (AL) and R01EY030668 (AL), P30 core grants EY002162 (UCSF) and P30EY016665 (UW-Madison), the Research to Prevent Blindness/AMDF Catalyst Award for novel approaches to AMD (AL), the BrightFocus Foundation Lorraine Maresca award for Innovative research in AMD M2021020I (AL), Reeves Foundation award for AMD (AL), All May See Foundation Postdoctoral Grant Award (LXT) and National Eye Institute Diversity Supplement R01EY030668S1 (NLC). We thank Jayanta Debnath for the GFP-LC3 mice and Haoxing Xu for the TRPML1 inhibitor MLSI3.

Inclusion and diversity

We support inclusive, diverse, and equitable conduct of research. One or more of the authors of this paper self-identifies as an underrepresented ethnic minority in science. One or more of the authors of this paper received support from a program designed to increase minority representation in science.

References

1. Caceres PS, and Rodriguez-Boulan E (2020). Retinal pigment epithelium polarity in health and blinding diseases. Curr Opin Cell Biol 62, 37–45. 10.1016/j.ceb.2019.08.001. [PubMed: 31518914]
2. Lakkaraju A, Umapathy A, Tan LX, Daniele L, Philp NJ, Boesze-Battaglia K, and Williams DS (2020). The cell biology of the retinal pigment epithelium. Progress in Retinal and Eye Research, 100846. 10.1016/j.preteyeres.2020.100846. [PubMed: 32105772]
3. Freeman S, and Grinstein S (2021). Promoters and Antagonists of Phagocytosis: A Plastic and Tunable Response. Annu Rev Cell Dev Biol 37, 89–114. 10.1146/annurev-cellbio-120219-055903. [PubMed: 34152790]
4. Umapathy A, Torten G, Paniagua AE, Chung J, Tomlinson M, Lim C, and Williams DS (2023). Spatiotemporal live-cell analysis of photoreceptor outer segment membrane ingestion by the retinal pigment epithelium reveals actin-regulated scission. J Neurosci. 10.1523/jneurosci.1726-22.2023.
5. Finnemann SC, Bonilha VL, Marmorstein AD, and Rodriguez-Boulan E (1997). Phagocytosis of rod outer segments by retinal pigment epithelial cells requires alpha(v)beta5 integrin for binding but not for internalization. Proc Natl Acad Sci U S A 94, 12932–12937. [PubMed: 9371778]
6. Nandrot EF, Anand M, Almeida D, Atabai K, Sheppard D, and Finnemann SC (2007). Essential role for MFG-E8 as ligand for alphavbeta5 integrin in diurnal retinal phagocytosis. Proc Natl Acad Sci U S A 104, 12005–12010. 10.1073/pnas.0704756104. [PubMed: 17620600]
7. Ruggiero L, Connor MP, Chen J, Langen R, and Finnemann SC (2012). Diurnal, localized exposure of phosphatidylserine by rod outer segment tips in wild-type but not Itgb5−/− or Mfge8−/− mouse retina. Proc Natl Acad Sci U S A 109, 8145–8148. 10.1073/pnas.1121101109. [PubMed: 22566632]
8. La Cunza N, Tan LX, Thamban T, Germer CJ, Rathnasamy G, Toops KA, and Lakkaraju A (2021). Mitochondria-dependent phase separation of disease-relevant proteins drives pathological features of age-related macular degeneration. JCI Insight 6. 10.1172/jci.insight.142254.
9. El-Asrag ME, Sergouniotis PI, McKibbin M, Plagnol V, Sheridan E, Waseem N, Abdelhamed Z, McKeefry D, Van Schil K, Poulter JA, et al. (2015). Biallelic mutations in the autophagy regulator DRAM2 cause retinal dystrophy with early macular involvement. Am J Hum Genet 96, 948–954. 10.1016/j.ajhg.2015.04.006. [PubMed: 25983245]
10. Mitter SK, Song C, Qi X, Mao H, Rao H, Akin D, Lewin A, Grant M, Dunn W Jr., Ding J, et al. (2014). Dysregulated autophagy in the RPE is associated with increased susceptibility to oxidative stress and AMD. Autophagy 10, 1989–2005. 10.4161/auto.36184. [PubMed: 25484094]
11. Kaur G, Tan LX, Rathnasamy G, La Cunza NR, Germer CJ, Toops KA, Fernandes M, Blenkinsop TA, and Lakkaraju A (2018). Aberrant early endosome biogenesis mediates complement activation in the retinal pigment epithelium in models of macular degeneration. Proc Natl Acad Sci U S A 115, 9014–9019. [PubMed: 30126999]
12. Toops KA, Tan LX, Jiang Z, Radu R, and Lakkaraju A (2015). Cholesterol-mediated activation of acid sphingomyelinase disrupts autophagy in the retinal pigment epithelium. Mol Biol Cell 26:1–14. [PubMed: 25378587]
13. Obin MS, Jahngen-Hodge J, Nowell T, and Taylor A (1996). Ubiquitinylation and ubiquitin-dependent proteolysis in vertebrate photoreceptors (rod outer segments). Evidence for ubiquitinylation of Gt and rhodopsin. J Biol Chem 271, 14473–14484. 10.1074/jbc.271.24.14473. [PubMed: 8662797]
14. He F, Wollscheid HP, Nowicka U, Biancospino M, Valentini E, Ehlinger A, Acconcia F, Magistrati E, Polo S, and Walters KJ (2016). Myosin VI Contains a Compact Structural Motif that Binds to Ubiquitin Chains. Cell Rep 14, 2683–2694. 10.1016/j.celrep.2016.01.079. [PubMed: 26971995]
15. Ripoll L, Heiligenstein X, Hurbain I, Domingues L, Figon F, Petersen KJ, Dennis MK, Houdusse A, Marks MS, Raposo G, et al. (2018). Myosin VI and branched actin filaments mediate membrane constriction and fission of melanosomal tubule carriers. J Cell Biol 217, 2709–2726. 10.1083/jcb.201709055. [PubMed: 29875258]
16. Lewis TR, Kundinger SR, Link BA, Insinna C, and Besharse JC (2018). Kif17 phosphorylation regulates photoreceptor outer segment turnover. BMC Cell Biol 19, 25. 10.1186/s12860-018-0177-9. [PubMed: 30458707]

17. Sundaramoorthy V, Walker AK, Tan V, Fifita JA, McCann EP, Williams KL, Blair IP, Guillemin GJ, Farg MA, and Atkin JD (2015). Defects in optineurin- and myosin VI-mediated cellular trafficking in amyotrophic lateral sclerosis. Hum Mol Genet 24, 3830–3846. 10.1093/hmg/ddv126. [PubMed: 25859013]

18. Sahlender DA, Roberts RC, Arden SD, Spudich G, Taylor MJ, Luzio JP, Kendrick-Jones J, and Buss F (2005). Optineurin links myosin VI to the Golgi complex and is involved in Golgi organization and exocytosis. J Cell Biol 169, 285–295. 10.1083/jcb.200501162. [PubMed: 15837803]

19. Hazim RA, and Williams DS (2018). Cell Culture Analysis of the Phagocytosis of Photoreceptor Outer Segments by Primary Mouse RPE Cells. Methods Mol Biol 1753, 63–71. 10.1007/978-1-4939-7720-8_4. [PubMed: 29564781]

20. Wagner W, Lippmann K, Heisler FF, Gromova KV, Lombino FL, Roesler MK, Pechmann Y, Hornig S, Schweizer M, Polo S, et al. (2019). Myosin VI Drives Clathrin-Mediated AMPA Receptor Endocytosis to Facilitate Cerebellar Long-Term Depression. Cell reports 28, 11–20.e19. 10.1016/j.celrep.2019.06.005. [PubMed: 31269433]

21. Brooks AB, Humphreys D, Singh V, Davidson AC, Arden SD, Buss F, and Koronakis V (2017). MYO6 is targeted by Salmonella virulence effectors to trigger PI3-kinase signaling and pathogen invasion into host cells. Proc Natl Acad Sci U S A 114, 3915–3920. 10.1073/pnas.1616418114. [PubMed: 28348208]

22. Yu B, Egbejimi A, Dharmat R, Xu P, Zhao Z, Long B, Miao H, Chen R, Wensel TG, Cai J, et al. (2018). Phagocytosed photoreceptor outer segments activate mTORC1 in the retinal pigment epithelium. Sci Signal 11. 10.1126/scisignal.aag3315.

23. Schubert T, Gleiser C, Heiduschka P, Franz C, Nagel-Wolfrum K, Sahaboglu A, Weisschuh N, Eske G, Rohbock K, Rieger N, et al. (2015). Deletion of myosin VI causes slow retinal optic neuropathy and age-related macular degeneration (AMD)-relevant retinal phenotype. Cell Mol Life Sci 72, 3953–3969. 10.1007/s00018-015-1913-3. [PubMed: 25939269]

24. Ryan TA, and Tumbarello DA (2018). Optineurin: A Coordinator of Membrane-Associated Cargo Trafficking and Autophagy. Front Immunol 9, 1024. 10.3389/fimmu.2018.01024. [PubMed: 29867991]

25. Wong YC, and Holzbaur EL (2014). Optineurin is an autophagy receptor for damaged mitochondria in parkin-mediated mitophagy that is disrupted by an ALS-linked mutation. Proc Natl Acad Sci U S A 111, E4439–4448. 10.1073/pnas.1405752111. [PubMed: 25294927]

26. Gao J, Ohtsubo M, Hotta Y, and Minoshima S (2014). Oligomerization of optineurin and its oxidative stress- or E50K mutation-driven covalent cross-linking: possible relationship with glaucoma pathology. PLoS One 9, e101206. 10.1371/journal.pone.0101206. [PubMed: 24983867]

27. Fang EF, Hou Y, Palikaras K, Adriaanse BA, Kerr JS, Yang B, Lautrup S, Hasan-Olive MM, Caponio D, Dan X, et al. (2019). Mitophagy inhibits amyloid-beta and tau pathology and reverses cognitive deficits in models of Alzheimer's disease. Nat Neurosci 22, 401–412. 10.1038/s41593-018-0332-9. [PubMed: 30742114]

28. Booty LM, Gawel JM, Cvetko F, Caldwell ST, Hall AR, Mulvey JF, James AM, Hinchy EC, Prime TA, Arndt S, et al. (2019). Selective Disruption of Mitochondrial Thiol Redox State in Cells and In Vivo. Cell Chem Biol 26, 449–461.e448. 10.1016/j.chembiol.2018.12.002. [PubMed: 30713096]

29. Söderberg O, Gullberg M, Jarvius M, Ridderstråle K, Leuchowius KJ, Jarvius J, Wester K, Hydbring P, Bahram F, Larsson LG, et al. (2006). Direct observation of individual endogenous protein complexes in situ by proximity ligation. Nat Methods 3, 995–1000. 10.1038/nmeth947. [PubMed: 17072308]

30. Heckmann BL, and Green DR (2019). LC3-associated phagocytosis at a glance. J Cell Sci 132. 10.1242/jcs.222984.

31. Kim JY, Zhao H, Martinez J, Doggett TA, Kolesnikov AV, Tang PH, Ablonczy Z, Chan CC, Zhou Z, Green DR, et al. (2013). Noncanonical autophagy promotes the visual cycle. Cell 154, 365–376. 10.1016/j.cell.2013.06.012. [PubMed: 23870125]

32. Frost LS, Lopes VS, Bragin A, Reyes-Reveles J, Brancato J, Cohen A, Mitchell CH, Williams DS, and Boesze-Battaglia K (2014). The Contribution of Melanoregulin to Microtubule-Associated Protein 1 Light Chain 3 (LC3) Associated Phagocytosis in Retinal Pigment Epithelium. Mol Neurobiol. 10.1007/s12035-014-8920-5.

33. Dhingra A, Bell BA, Peachey NS, Daniele LL, Reyes-Reveles J, Sharp RC, Jun B, Bazan NG, Sparrow JR, Kim HJ, et al. (2018). Microtubule-Associated Protein 1 Light Chain 3B, (LC3B) Is Necessary to Maintain Lipid-Mediated Homeostasis in the Retinal Pigment Epithelium. Front Cell Neurosci 12, 351. 10.3389/fncel.2018.00351. [PubMed: 30349463]
34. Wavre-Shapton ST, Meschede IP, Seabra MC, and Futter CE (2014). Phagosome maturation during endosome interaction revealed by partial rhodopsin processing in retinal pigment epithelium. J Cell Sci 127, 3852–3861. 10.1242/jcs.154757. [PubMed: 25074813]
35. Dooley HC, Wilson MI, and Tooze SA (2015). WIPI2B links PtdIns3P to LC3 lipidation through binding ATG16L1. Autophagy 11, 190–191. 10.1080/15548627.2014.996029. [PubMed: 25629784]
36. Bansal M, Moharir SC, Sailasree SP, Sirohi K, Sudhakar C, Sarathi DP, Lakshmi BJ, Buono M, Kumar S, and Swarup G (2018). Optineurin promotes autophagosome formation by recruiting the autophagy-related Atg12–5-16L1 complex to phagophores containing the Wipi2 protein. J Biol Chem 293, 132–147. 10.1074/jbc.M117.801944. [PubMed: 29133525]
37. Wild P, Farhan H, McEwan DG, Wagner S, Rogov VV, Brady NR, Richter B, Korac J, Waidmann O, Choudhary C, et al. (2011). Phosphorylation of the autophagy receptor optineurin restricts Salmonella growth. Science 333, 228–233. 10.1126/science.1205405. [PubMed: 21617041]
38. Padman BS, Nguyen TN, Uoselis L, Skulsuppaisarn M, Nguyen LK, and Lazarou M (2019). LC3/GABARAPs drive ubiquitin-independent recruitment of Optineurin and NDP52 to amplify mitophagy. Nat Commun 10, 408. 10.1038/s41467-019-08335-6. [PubMed: 30679426]
39. Hattula K, and Peränen J (2000). FIP-2, a coiled-coil protein, links Huntingtin to Rab8 and modulates cellular morphogenesis. Curr Biol 10, 1603–1606. 10.1016/s0960-9822(00)00864-2. [PubMed: 11137014]
40. Lee H, Flynn R, Sharma I, Haberman E, Carling PJ, Nicholls FJ, Stegmann M, Vowles J, Haenseler W, Wade-Martins R, et al. (2020). LRRK2 Is Recruited to Phagosomes and Co-recruits RAB8 and RAB10 in Human Pluripotent Stem Cell-Derived Macrophages. Stem Cell Reports 14, 940–955. 10.1016/j.stemcr.2020.04.001. [PubMed: 32359446]
41. Bloom GS, Schoenfeld TA, and Vallee RB (1984). Widespread distribution of the major polypeptide component of MAP 1 (microtubule-associated protein 1) in the nervous system. J Cell Biol 98, 320–330. 10.1083/jcb.98.1.320. [PubMed: 6368569]
42. Jiang M, Esteve-Rudd J, Lopes VS, Diemer T, Lillo C, Rump A, and Williams DS (2015). Microtubule motors transport phagosomes in the RPE, and lack of KLC1 leads to AMD-like pathogenesis. J Cell Biol 210, 595–611. 10.1083/jcb.201410112. [PubMed: 26261180]
43. Harrison RE, Bucci C, Vieira OV, Schroer TA, and Grinstein S (2003). Phagosomes fuse with late endosomes and/or lysosomes by extension of membrane protrusions along microtubules: role of Rab7 and RILP. Mol Cell Biol 23, 6494–6506. 10.1128/mcb.23.18.6494-6506.2003. [PubMed: 12944476]
44. Martinez J, Almendinger J, Oberst A, Ness R, Dillon CP, Fitzgerald P, Hengartner MO, and Green DR (2011). Microtubule-associated protein 1 light chain 3 alpha (LC3)-associated phagocytosis is required for the efficient clearance of dead cells. Proc Natl Acad Sci U S A 108, 17396–17401. 10.1073/pnas.1113421108. [PubMed: 21969579]
45. Romao S, Gasser N, Becker AC, Guhl B, Bajagic M, Vanoaica D, Ziegler U, Roesler J, Dengjel J, Reichenbach J, et al. (2013). Autophagy proteins stabilize pathogen-containing phagosomes for prolonged MHC II antigen processing. J Cell Biol 203, 757–766. 10.1083/jcb.201308173. [PubMed: 24322427]
46. Palmieri M, Impey S, Kang H, di Ronza A, Pelz C, Sardiello M, and Ballabio A (2011). Characterization of the CLEAR network reveals an integrated control of cellular clearance pathways. Hum Mol Genet 20, 3852–3866. 10.1093/hmg/ddr306. [PubMed: 21752829]
47. Settembre C, Di Malta C, Polito VA, Garcia Arencibia M, Vetrini F, Erdin S, Erdin SU, Huynh T, Medina D, Colella P, et al. (2011). TFEB links autophagy to lysosomal biogenesis. Science 332, 1429–1433. 10.1126/science.1204592. [PubMed: 21617040]
48. Xu Y, Du S, Marsh JA, Horie K, Sato C, Ballabio A, Karch CM, Holtzman DM, and Zheng H (2021). TFEB regulates lysosomal exocytosis of tau and its loss of function exacerbates tau pathology and spreading. Mol Psychiatry 26, 5925–5939. 10.1038-/s41380020-0738-0. [PubMed: 32366951]

49. Martina JA, Chen Y, Gucek M, and Puertollano R (2012). MTORC1 functions as a transcriptional regulator of autophagy by preventing nuclear transport of TFEB. Autophagy 8, 903–914. 10.4161/auto.19653. [PubMed: 22576015]
50. Gray MA, Choy CH, Dayam RM, Ospina-Escobar E, Somerville A, Xiao X, Ferguson SM, and Botelho RJ (2016). Phagocytosis Enhances Lysosomal and Bactericidal Properties by Activating the Transcription Factor TFEB. Curr Biol 26, 1955–1964. 10.1016/j.cub.2016.05.070. [PubMed: 27397893]
51. Medina DL, Di Paola S, Peluso I, Armani A, De Stefani D, Venditti R, Montefusco S, Scotto-Rosato A, Prezioso C, Forrester A, et al. (2015). Lysosomal calcium signalling regulates autophagy through calcineurin and TFEB. Nat Cell Biol 17, 288–299. 10.1038/ncb3114. [PubMed: 25720963]
52. Li X, Rydzewski N, Hider A, Zhang X, Yang J, Wang W, Gao Q, Cheng X, and Xu H (2016). A molecular mechanism to regulate lysosome motility for lysosome positioning and tubulation. Nat Cell Biol 18, 404–417. 10.1038/ncb3324. [PubMed: 26950892]
53. Audesse AJ, Dhakal S, Hassell LA, Gardell Z, Nemtsova Y, and Webb AE (2019). FOXO3 directly regulates an autophagy network to functionally regulate proteostasis in adult neural stem cells. PLoS Genet 15, e1008097. 10.1371/journal.pgen.1008097. [PubMed: 30973875]
54. Tumbarello DA, Manna PT, Allen M, Bycroft M, Arden SD, Kendrick-Jones J, and Buss F (2015). The Autophagy Receptor TAX1BP1 and the Molecular Motor Myosin VI Are Required for Clearance of Salmonella Typhimurium by Autophagy. PLoS Pathog 11, e1005174. 10.1371/journal.ppat.1005174. [PubMed: 26451915]
55. Morriswood B, Ryzhakov G, Puri C, Arden SD, Roberts R, Dendrou C, Kendrick-Jones J, and Buss F (2007). T6BP and NDP52 are myosin VI binding partners with potential roles in cytokine signalling and cell adhesion. J Cell Sci 120, 2574–2585. 10.1242/jcs.007005. [PubMed: 17635994]
56. Kruppa AJ, Kishi-Itakura C, Masters TA, Rorbach JE, Grice GL, Kendrick-Jones J, Nathan JA, Minczuk M, and Buss F (2018). Myosin VI-Dependent Actin Cages Encapsulate Parkin-Positive Damaged Mitochondria. Dev Cell 44, 484–499.e486. 10.1016/j.devcel.2018.01.007. [PubMed: 29398621]
57. Zhao C, Yasumura D, Li X, Matthes M, Lloyd M, Nielsen G, Ahern K, Snyder M, Bok D, Dunaief JL, et al. (2011). mTOR-mediated dedifferentiation of the retinal pigment epithelium initiates photoreceptor degeneration in mice. J Clin Invest 121, 369–383. 10.1172/JCI44303. [PubMed: 21135502]
58. Yu B, Xu P, Zhao Z, Cai J, Sternberg P, and Chen Y (2014). Subcellular distribution and activity of mechanistic target of rapamycin in aged retinal pigment epithelium. Invest Ophthalmol Vis Sci 55, 8638–8650. 10.1167/iovs.14-14758. [PubMed: 25491300]
59. Cai J, Litwin C, Cheng R, Ma JX, and Chen Y (2022). DARPP32, a target of hyperactive mTORC1 in the retinal pigment epithelium. Proc Natl Acad Sci U S A 119, e2207489119. 10.1073/pnas.2207489119. [PubMed: 35939707]
60. Burns JC, Cotleur B, Walther DM, Bajrami B, Rubino SJ, Wei R, Franchimont N, Cotman SL, Ransohoff RM, and Mingueneau M (2020). Differential accumulation of storage bodies with aging defines discrete subsets of microglia in the healthy brain. Elife 9. 10.7554/eLife.57495.
61. Ulland TK, Song WM, Huang SC, Ulrich JD, Sergushichev A, Beatty WL, Loboda AA, Zhou Y, Cairns NJ, Kambal A, et al. (2017). TREM2 Maintains Microglial Metabolic Fitness in Alzheimer's Disease. Cell 170, 649–663 e613. 10.1016/j.cell.2017.07.023. [PubMed: 28802038]
62. Berglund R, Guerreiro-Cacais AO, Adzemovic MZ, Zeitelhofer M, Lund H, Ewing E, Ruhrmann S, Nutma E, Parsa R, Thessen-Hedreul M, et al. (2020). Microglial autophagy-associated phagocytosis is essential for recovery from neuroinflammation. Sci Immunol 5. 10.1126/sciimmunol.abb5077.
63. Petkau TL, Kosior N, de Asis K, Connolly C, and Leavitt BR (2017). Selective depletion of microglial progranulin in mice is not sufficient to cause neuronal ceroid lipofuscinosis or neuroinflammation. J Neuroinflammation 14, 225. 10.1186/s12974-017-1000-9. [PubMed: 29149899]

64. Spandidos A, Wang X, Wang H, and Seed B (2010). PrimerBank: a resource of human and mouse PCR primer pairs for gene expression detection and quantification. Nucleic Acids Res 38, D792–799. 10.1093/nar/gkp1005. [PubMed: 19906719]

65. Farmer DT, Nathan S, Finley JK, Shengyang Yu K, Emmerson E, Byrnes LE, Sneddon JB, McManus MT, Tward AD, and Knox SM (2017). Defining epithelial cell dynamics and lineage relationships in the developing lacrimal gland. Development 144, 2517–2528. 10.1242/dev.150789. [PubMed: 28576768]

66. Park BC, Shen X, Samaraweera M, and Yue BY (2006). Studies of optineurin, a glaucoma gene: Golgi fragmentation and cell death from overexpression of wild-type and mutant optineurin in two ocular cell types. Am J Pathol 169, 1976–1989. 10.2353/ajpath.2006.060400. [PubMed: 17148662]

67. Turturro S, Shen X, Shyam R, Yue BY, and Ying H (2014). Effects of mutations and deletions in the human optineurin gene. Springerplus 3, 99. 10.1186/2193-1801-3-99. [PubMed: 24683533]

68. Roczniak-Ferguson A, Petit CS, Froehlich F, Qian S, Ky J, Angarola B, Walther TC, and Ferguson SM (2012). The transcription factor TFEB links mTORC1 signaling to transcriptional control of lysosome homeostasis. Sci Signal 5, ra42. 10.1126/scisignal.2002790. [PubMed: 22692423]

69. Toops KA, Tan LX, and Lakkaraju A (2014). A detailed three-step protocol for live imaging of intracellular traffic in polarized primary porcine RPE monolayers. Experimental eye research 124, 74–85. 10.1016/j.exer.2014.05.003. [PubMed: 24861273]

70. Parinot C, Rieu Q, Chatagnon J, Finnemann SC, and Nandrot EF (2014). Large-scale purification of porcine or bovine photoreceptor outer segments for phagocytosis assays on retinal pigment epithelial cells. J Vis Exp. 10.3791/52100.

71. Toops KA, Tan LX, and Lakkaraju A (2014). A detailed three-step protocol for live imaging of intracellular traffic in polarized primary porcine RPE monolayers. Exp Eye Res 124C, 74–85.

72. Kaur G, Tan LX, Rathnasamy G, La Cunza N, Germer CJ, Toops KA, Fernandes M, Blenkinsop TA, and Lakkaraju A (2018). Aberrant early endosome biogenesis mediates complement activation in the retinal pigment epithelium in models of macular degeneration. Proc Natl Acad Sci U S A 115, 9014–9019. 10.1073/pnas.1805039115. [PubMed: 30126999]

73. Tan LX, Toops KA, and Lakkaraju A (2016). Protective responses to sublytic complement in the retinal pigment epithelium. Proc Natl Acad Sci U S A 113, 8789–8794. 10.1073/pnas.1523061113. [PubMed: 27432952]

74. Love MI, Huber W, and Anders S (2014). Moderated estimation of fold change and dispersion for RNA-seq data with DESeq2. Genome Biol 15, 550. 10.1186/s13059-014-0550-8. [PubMed: 25516281]

Highlights

- Optineurin and myosin 6 execute trogocytosis of outer segment tips by the RPE
- Optineurin-LC3 interactions regulate phagosome maturation and TFEB activation
- Circadian TFEB dynamics are maintained even under conditions of impaired autophagy
- Distinct regulation of clearance pathways preserves metabolic fitness of the retina

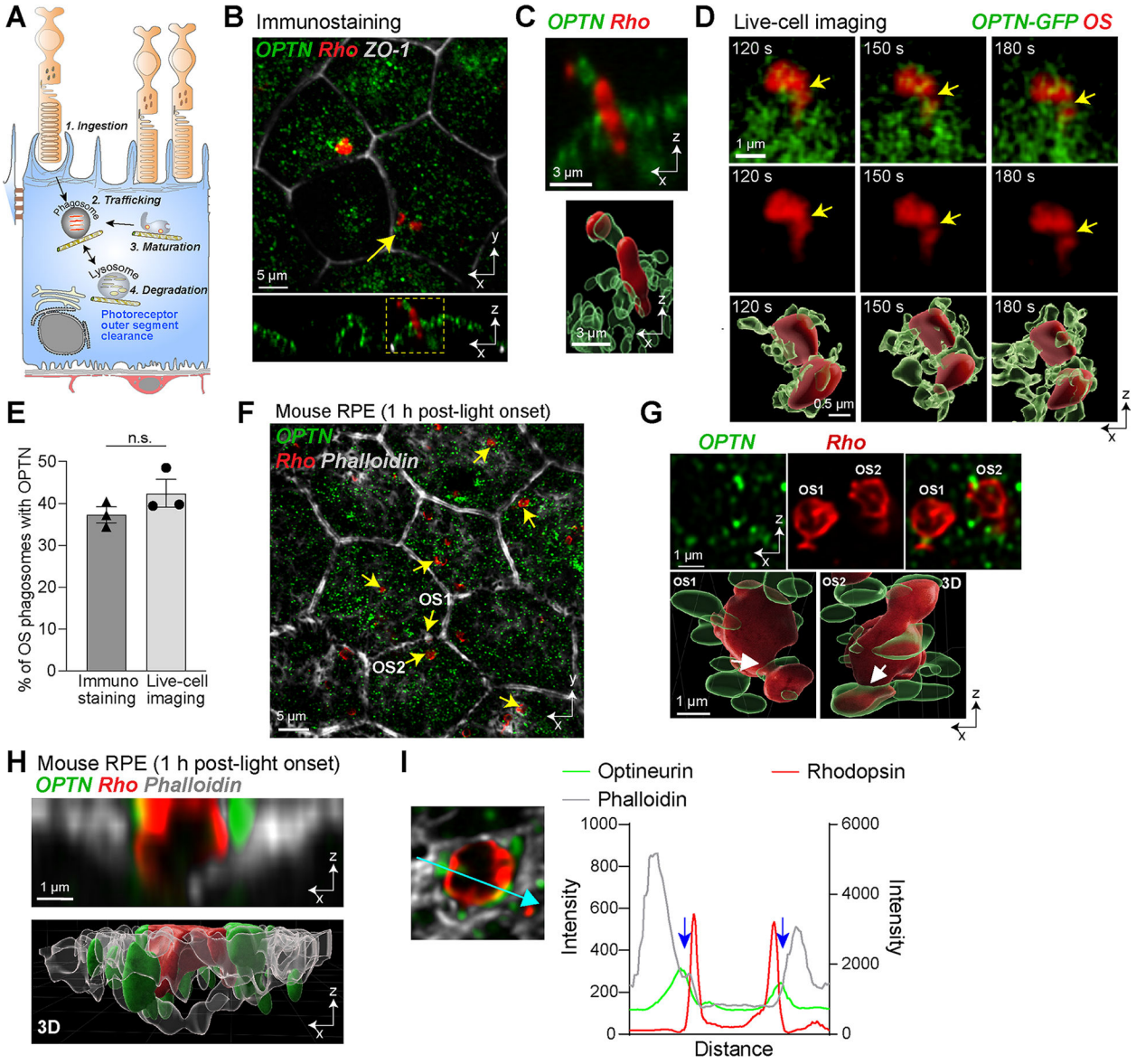

Figure 1. Scissioning of photoreceptor outer segments is facilitated by optineurin.

(**A**) Four major steps in the phagocytosis and clearance of photoreceptor outer segments by the RPE. (**B**) Representative en face and x-z images of polarized primary RPE monolayers fed outer segments (OS) for 30 min and immunostained for optineurin (green) and rhodopsin (red). ZO-1 (gray) demarcates cell boundaries. Yellow arrow: outer segment interacting with optineurin. Scale bar: 5 µm. (**C**) High-magnification x-z image and 3D-reconstruction of optineurin-outer segment interaction shown in yellow dashed square in B. Scale bars: 3 µm. (**D**) Stills from live imaging of polarized primary RPE expressing optineurin-GFP (green) fed Alexa647-labeled outer segments (OS, red) for 30 min. Arrows point to sites of scission events. (**E**) Percent optineurin-positive outer segment phagosomes in primary RPE after 30 min measured by immunofluorescence or by live imaging. Mean ± SEM, n = 3 independent experiments. n.s., not significant by Welch's t-test. Approximately 1,200 phagosomes in ~300 cells were analyzed for immunofluorescence and ~150 phagosomes

in 30 cells for live imaging. (**F**) Representative immunofluorescence image of mouse RPE flatmount stained 1 h after light onset for optineurin (green) and rhodopsin (red). Cell boundaries are demarcated by actin (phalloidin, gray). Yellow arrows: optineurin-positive phagosomes. Scale bar = 5 μm. (**G**) High-magnification split channel images and 3D-reconstruction of optineurin-positive outer segment phagosomes labeled OS1 and OS2 in F. White arrow in OS1: optineurin localized to a putative outer segment scission site. Arrow in OS2: optineurin at the edges of the phagosome. Scale bars = 1 μm. (**H**) Representative high-magnification (top) and 3D-reconstruction of optineurin (green) associating with an outer segment (rhodopsin, red) in the phagocytic cup in mouse RPE flatmounts at 1 h after light onset. Gray: actin stain phalloidin. Scale bar = 1 μm. (**I**) Intensity profile of optineurin along the axis marked by white arrow in the inset. Blue arrows: optineurin intensity peaks at the edges of an outer segment phagosome. Also see Figure S1 and Video S1.

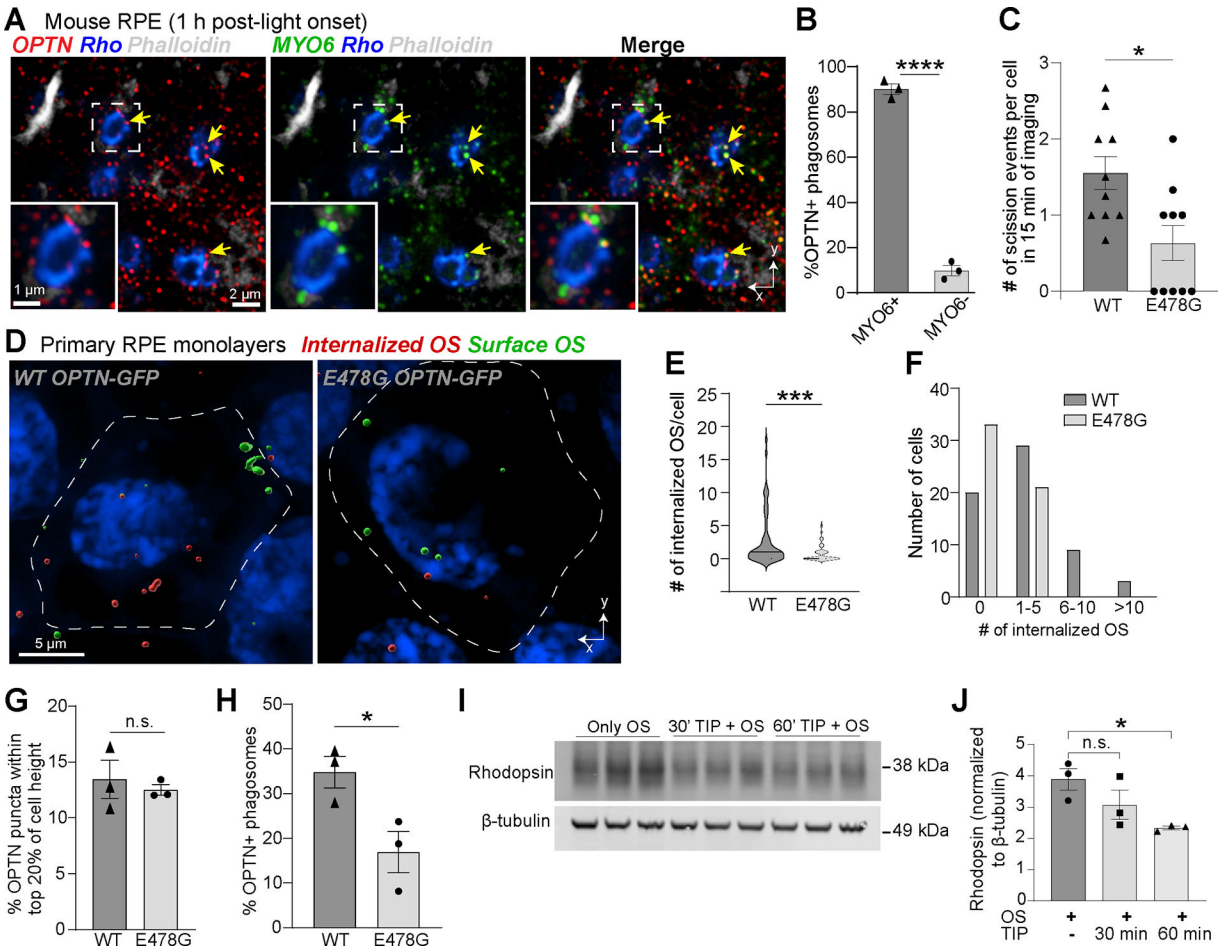

Figure 2. Optineurin-MYO6 interaction promotes outer segment scissioning.

(**A**) Representative immunofluorescence image of mouse RPE flatmount stained 1 h after light onset for OPTN (red), MYO6 (green), and rhodopsin (blue). Yellow arrows: co-localization of proteins. Insets: enlarged views of the phagosome in the white box. (**B**) Percent optineurin-positive phagosomes that are either positive or negative for MYO6. Mean ± SEM, n = 3 mice. **** $p < 0.0001$ by t-test. Approximately 2,000 phagosomes in ~300 cells were analyzed. (**C**) Number of outer segment scission events per cell during the 15-min imaging period in RPE expressing either WT or E478G mutant optineurin quantified from live imaging. Mean ± SEM, * $p < 0.05$ by Welch's t-test. n = 10 cells per condition, three independent experiments. (**D**) Surface reconstruction of internalized (red) and uninternalized (green) outer segments in primary RPE expressing GFP-tagged WT or E478G mutant OPTN. Transfected cells are demarcated by dashed lines. (**E**) Violin plot of number of internalized outer segments (OS) per cell in primary RPE expressing either WT-OPTN or E478G-OPTN. Mean ± SEM, *** $p < 0.0005$ by Welch's t-test. n = 3 independent experiments, ~60 cells/condition. (**F**) Frequency distribution of number of cells expressing either WT-OPTN or E478G-OPTN with outer segments. (**G**) Percent of total WT-OPTN and E478G-OPTN located apically (top 20% of cell height). Mean ± SEM, n = 3 independent experiments, ~45 cells/condition. n.s. by Welch's t-test. (**H**) Percent of optineurin-positive outer segment phagosomes in primary RPE expressing either

WT-OPTN or E478G-OPTN. * $p < 0.05$ by Welch's t-test. Mean ± SEM, n = 3 independent experiments, ~60 cells/condition. (**I**) Immunoblot of outer segment phagocytosis (rhodopsin) in primary RPE pre-treated or not with 2,4,6-triiodophenol (TIP) for 30 or 60 min followed by outer segment feeding (~40 OS/cell, 30 min). Loading control: β-tubulin. (**J**) Quantitation of (I). Mean ± SEM, n = 3 replicates/condition * $p < 0.05$ by one-way ANOVA with Dunnett's multiple comparisons test. Also see Figure S1 and Videos S1 and S2.

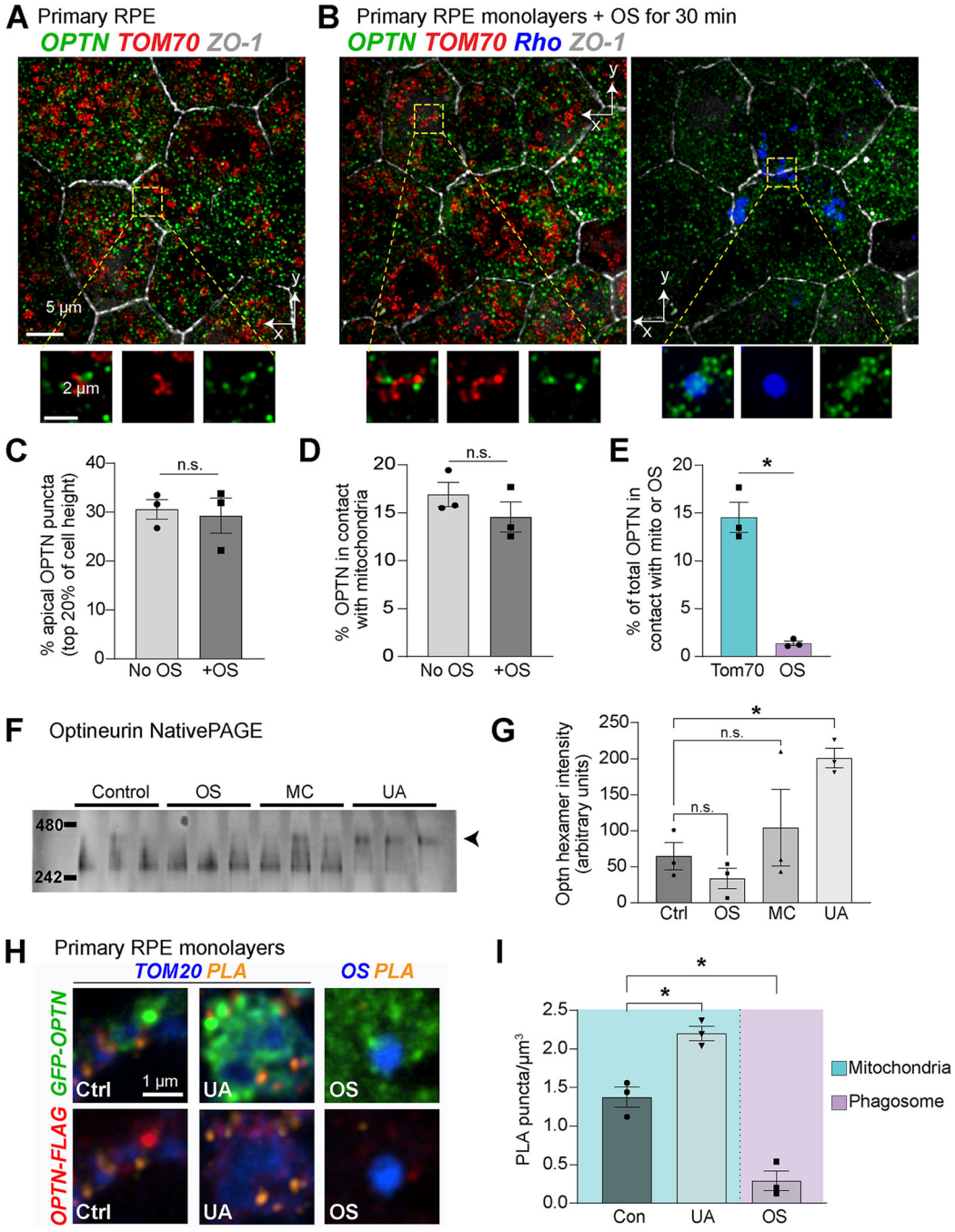

Figure 3. Oligomerization status of optineurin determines preferential association with phagosomes.

(**A**) Representative immunofluorescence images of optineurin (green) and TOM70 (red) in polarized primary RPE monolayers. (**B**) Optineurin (green) and TOM70 (red) immunofluorescence in primary RPE fed outer segments (rhodopsin, blue) for 30 min. ZO-1 is in gray. Scale bar: 5 µm. Lower panels in A & B show zoomed in split channel views of areas in yellow boxes. Scale bar: 2 µm. (**C**) Percent of apical optineurin (within top 20% of cell height) in primary RPE monolayers prior to and after outer segment feeding (~40

OS/cell, 30 min). (**D**) Percent of total optineurin colocalized with TOM70 mitochondria in primary RPE monolayers. (**E**) Percent of total optineurin on TOM70-positive mitochondria or on outer segment phagosomes in RPE fed outer segments for 30 min. For C-E, data are shown as Mean ± SEM, * $p < 0.05$ by Welch's t-test, n.s., not significant, n = 3 independent experiments, ~ 800 cells were analyzed per condition per experiment. (**F**) NativePAGE of RPE lysates immunoblotted for optineurin. Cells were either untreated or fed with outer segments (~40 OS/cell, 30 min), or treated with either mitoChlorodinitrobenzoic acid (MC, 5 μM, 30 min) or Urolithin A (UA, 100 μM, 24 h). Arrowhead: ~420 kD optineurin hexamers. (**G**) Quantitation of immunoblot in (F). Mean ± SEM, * $p < 0.05$, Brown-Forsythe and Welch's ANOVA test, n = 3 independent experiments. (**H**) Proximity ligation assay (PLA) of primary RPE expressing GFP- (green) and Flag-tagged (red) optineurin and treated as in (F). Cells were co-stained for TOM20 (blue, left panel) or rhodopsin (blue, right panel). (**I**) Quantitation of (H). Mean ± SEM. * $p < 0.05$, Brown-Forsythe and Welch's ANOVA test. n = ~50 cells/condition from 3 independent experiments. Also see Figure S2.

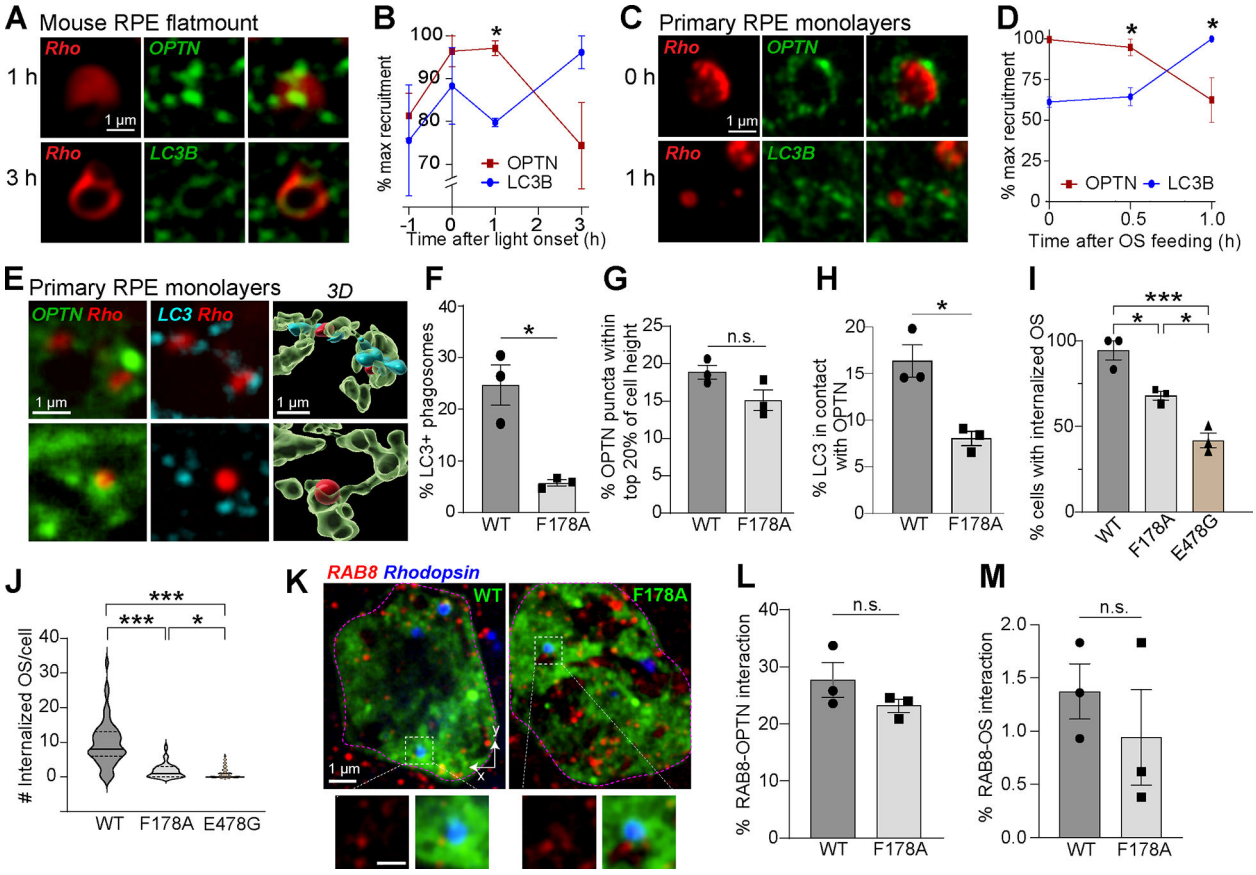

Figure 4. Optineurin recruits LC3 to nascent outer segment-containing phagosomes in the RPE.

(**A**) Representative high-magnification images of outer segment phagosomes in mouse RPE flatmounts stained for optineurin or LC3 (both green) and outer segment phagosomes (rhodopsin, red) at 1 h or 3 h after light onset. Scale bar: 1 µm. Corresponding full-field images with multiple RPE cells and phagosomes are shown in Figures S3A & S3B. (**B**) Percent optineurin- or LC3-positive phagosomes in mouse RPE flatmounts at −1, 0, 1, and 3 h after light onset. *, optineurin recruitment peaks at 1 h after light onset, Mean ± SEM, $p < 0.05$, two-way ANOVA with Sidak's multiple comparisons tests, n = 3 mice per timepoint, ~800 phagosomes per mouse per timepoint. (**C**) Representative high-magnification images of outer segment phagosomes in primary RPE monolayers stained for optineurin or LC3 (both green) and outer segment phagosomes (rhodopsin, red) at 0, 0.5 or 1 h chase in fresh medium after 30-min outer segment feeding. Scale bar: 1 µm. Corresponding full-field images are shown in Figures S3E & S3F. (**D**) Percent optineurin or LC3-positive outer segment phagosomes in (C). Peak recruitment of optineurin and LC3 occurs at 0 h and 1 h, respectively, after OS feeding. Mean ± SEM. * $p < 0.05$, two-way ANOVA with Sidak's multiple comparisons tests. n = 280 cells/condition from 3 independent experiments. (**E**) High-magnification images of *en face* and 3D reconstructions of LC3 (cyan) and rhodopsin (red) immunostaining in primary RPE monolayers expressing GFP-tagged WT or the F178A LIR mutant optineurin (green). Cells were fixed 1 h after outer segment phagocytosis, which is the time of peak LC3 recruitment seen in (D). Scale bars: 1 µm. See Figure S3H for full-field images. (**F**) Percent LC3-positive phagosomes at 1 h chase. (**G**) Percent of apical

GFP-optineurin (within top 20% of cell height) in cells expressing either WT or F178A constructs. (**H**) Percent of total LC3 in contact with optineurin. For F-H, Mean ± SEM, * p <0.05 by Welch's t-test, n = ~66 cells/condition from 3 independent experiments. (**I**) Percent cells with internalized outer segments in RPE expressing WT, F178A, or E478G optineurin constructs. Mean ± SEM. (**J**) Violin plot of internalized outer segments/cell. Median is indicated by solid lines and quartiles by dotted lines. For I and J, * $p < 0.05$, *** $p < 0.001$, by one-way ANOVA with Tukey's multiple comparisons test. n = ~50 cells/condition from 3 independent experiments. Also see Figure S3H & S3I. (**K**) Immunostaining for RAB8 (red) in primary RPE expressing WT or F178A optineurin (green) fed with ~40 OS/cell (blue) for 30 min. Cell boundaries marked with purple dashed lines. Scale bar: 2 μm. Insets show high-magnification views of regions in white boxes. Scale bar: 1 μm. Quantitation of (**L**) RAB8-optineurin and (**M**) RAB8-outer segment interactions from (K). Mean ± SEM, n = 25 cells/condition from 3 independent experiments. n.s. by Welch's t-test. Also see Figure S3.

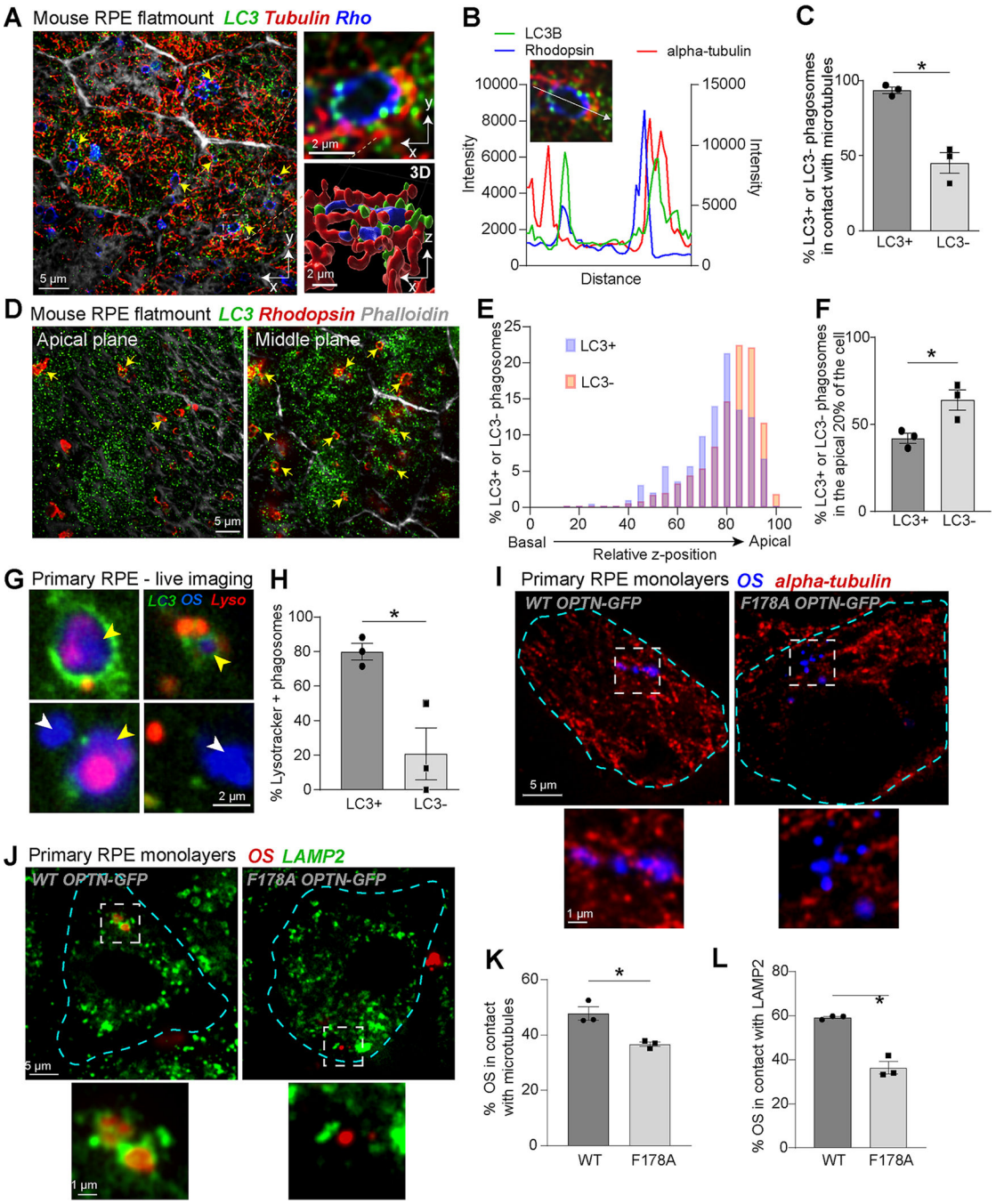

Figure 5. LC3 anchors phagosomes to microtubules and promotes phagosome-lysosome interactions.

(A) Representative full field views with high-magnification and 3D reconstruction of outer segment phagosomes (rhodopsin, blue), LC3 (green), and α-tubulin (red) in mouse RPE flatmounts at 1 h after light onset. **(B)** Intensity profile along the axis marked by white arrow in the inset. **(C)** Percent of LC3-positive or LC3-negative phagosomes that associate with microtubules. Mean ± SEM. * $p < 0.05$ Welch's t-test, ~ 400 phagosomes were quantified from 3 mice. **(D)** Single-plane images of LC3 (green), rhodopsin (red), and phalloidin (gray)

in mouse RPE flatmount corresponding to the apical and middle locations in the cell. **(E)** Frequency distribution of LC3+ and LC3− phagosome z-positions as a function of cell height. n = 3 mice. **(F)** Percent of apically localized LC3+ or LC3− phagosomes (within top 20% of cell height). Mean ± SEM, * $p < 0.05$ Welch's *t*-test. ~ 400 phagosomes were quantified from 3 mice. (**G**) Primary RPE monolayers expressing GFP-LC3 (green) fed outer segments (blue) for 30 min followed by 15 min lysotracker labeling (red). Yellow arrows: LC3-positive phagosomes; white arrows: LC3-negative phagosomes. Also see Video S3. (**H**) Quantification of interactions between lysosomes and LC3-positive or LC3-negative phagosomes from live imaging. Mean ± SEM. * $p < 0.05$ by Welch's *t*-test. n = 47 phagosomes from 15 cells, 3 independent experiments. Interactions between outer segment phagosomes (blue) and (**I**) microtubules (red) and (**J**) lysosomes (red) in primary RPE expressing WT or F178A (LIR mutant) OPTN. Transfected cells are demarcated by green dashed lines. Insets show enlarged view of boxed regions. (**K**) Quantification of phagosome-microtubule interactions from (**I**). Mean ± SEM. * $p < 0.05$ by Welch's *t*-test. n = ~120 phagosomes from ~35 cells per condition, 3 independent experiments. (**L**) Quantification of phagosome-lysosome interactions from (J). Mean ± SEM. * $p < 0.05$ by Welch's *t*-test. n = ~150 phagosomes from ~40 cells per condition, 3 independent experiments. Also see Video S3.

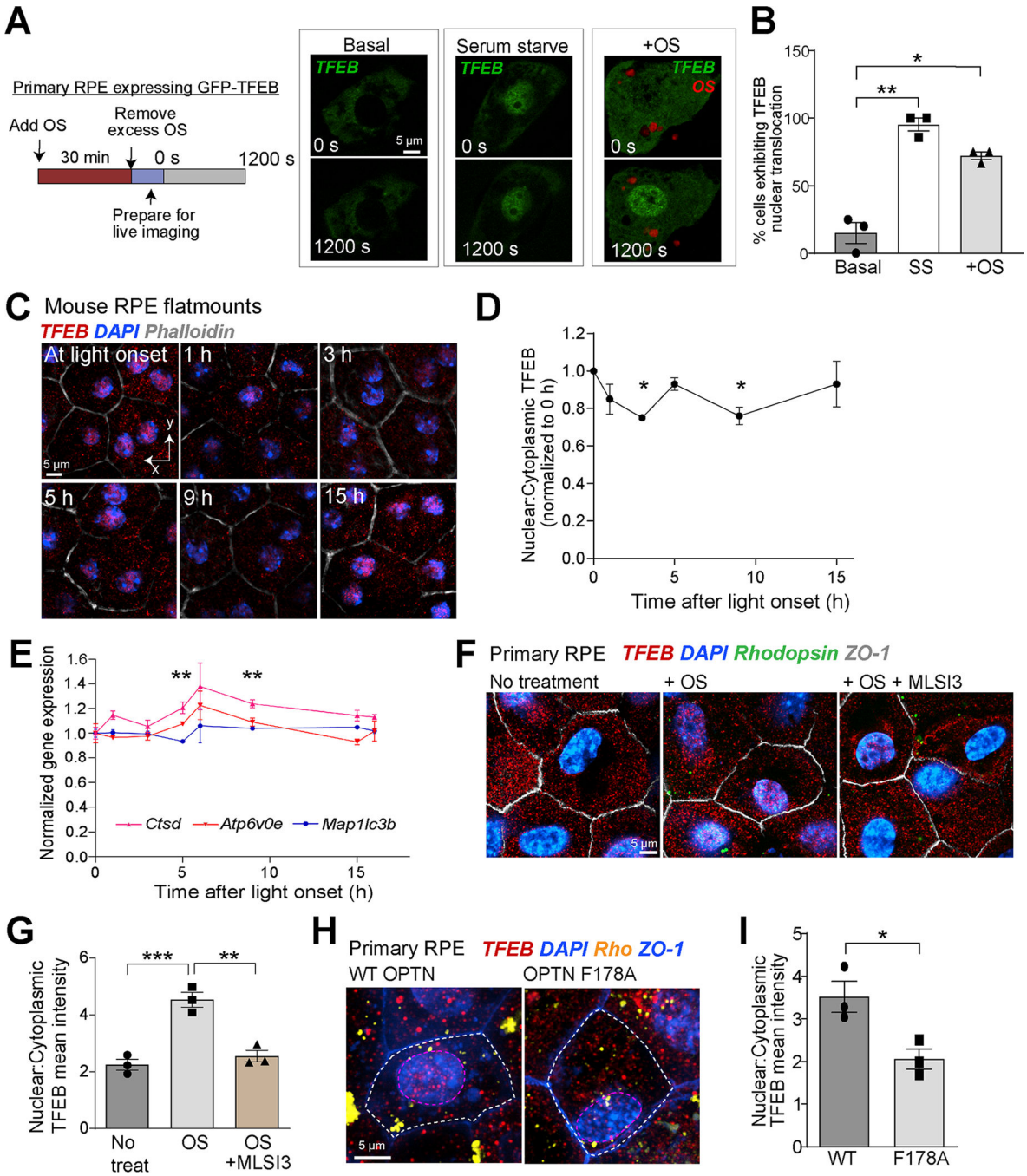

Figure 6. Outer segment phagocytosis induces TRPML1-mediated nuclear translocation of TFEB.

(**A**) Experimental design and stills at 0 and 1200 sec from live imaging of GFP-TFEB (green) dynamics in RPE under basal steady state conditions (Basal), after serum starvation (SS), or after outer segment phagocytosis (~40 OS/cell for 30 min). Scale bar: 5 µm. (**B**) Percent cells with nuclear GFP-TFEB in each condition from live imaging data in A. Mean ± SEM. * $p < 0.05$, ** $p < 0.01$ Brown-Forsythe and Welch ANOVA with Dunnett's T3 multiple comparisons test. n = 11–18 cells/condition from 3 independent experiments. (**C**)

Immunostaining of TFEB (red) in mouse RPE flatmounts harvested at 0, 1, 3, 5, 9, or 15 h after light onset. Scale bar: 5 μm. (**D**) Ratio of nuclear to cytoplasmic TFEB fluorescence in mouse RPE flatmounts from (D), normalized to the ratio at light onset. Mean ± SEM, * $p < 0.05$ one-way ANOVA with Tukey's multiple comparisons test, 3 mice/time point. (**E**) Transcript levels (FPKM) of selected TFEB targets at specific times after light onset from RNAseq analyses, normalized to expression levels at light onset. Mean ± SEM, ** $p_{adj} < 0.01$ for *Ctsd* by Wald test with Benjamini-Hochberg correction using DESeq2, 3 mice/time point. (**F**) Immunostaining of TFEB (red) and rhodopsin (green) in primary RPE monolayers treated or not with the TRPML1 inhibitor MLSI3 (25 μM, 1.5 h). Nuclei: blue (DAPI); ZO-1: gray. Scale bar: 5 μm. (**G**) Quantification of nuclear to cytoplasmic TFEB signal from (F). Mean ± SEM, ** $p < 0.01$ and *** $p < 0.001$, one-way ANOVA with Tukey's multiple comparisons test. n = 270 cells/condition from 3 independent experiments. (**H**) Immunostaining of TFEB (red) and rhodopsin (yellow) in primary RPE monolayers expressing GFP-tagged wildtype (WT) or F178A constructs fed OS for 30 min followed by 1.5 h incubation in fresh medium. Nuclei (purple circles) and cell boundaries (white dotted-lines) were identified by DAPI and ZO-1, respectively. Scale bar = 5 μm. (**I**) Quantification of (H). Mean ± SEM. * $p < 0.05$ Welch's *t*-test. n = ~40 cells/condition from 3 independent experiments. Also see Figure S4 and Videos S4–S6.

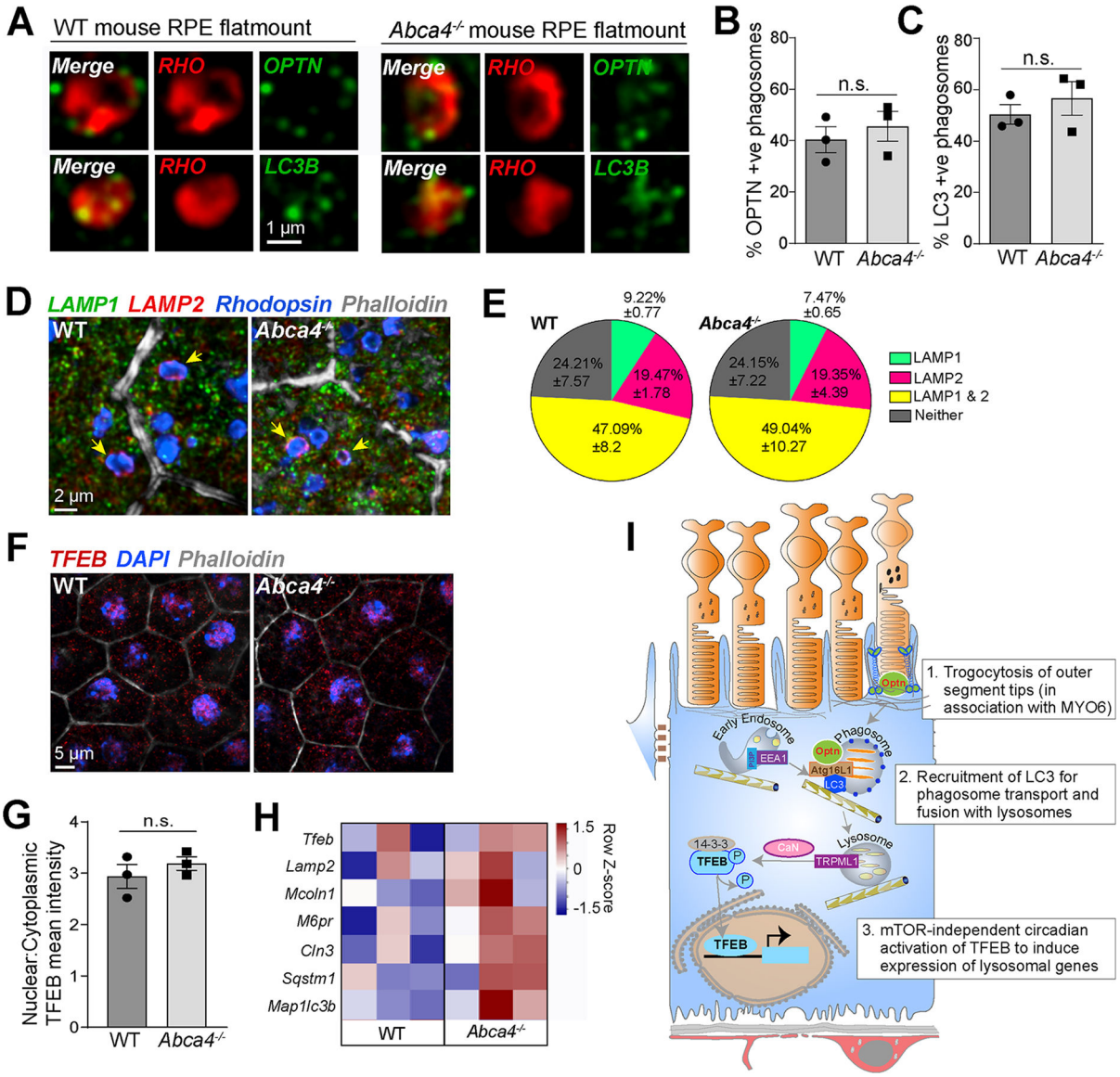

Figure 7. TFEB activation in response to outer segment phagocytosis is maintained under conditions of impaired autophagy.

(**A**) Representative high-magnification images of outer segment phagosomes (rhodopsin, red) and optineurin (green, top panel), and LC3 (green, lower panel) in 6-month-old WT and *Abca4*$^{-/-}$ mouse RPE flatmounts at 1 h (optineurin) and 3 h (LC3) after light onset corresponding to times of respective peak recruitment (see Figures 3 A and B). Scale bar: 1 µm. (**B**) and (**C**) Quantification of optineurin- or LC3-associated phagosomes as percentage of total phagosomes. (**D**) Representative immunofluorescence images of LAMP1 (green), LAMP2 (red), and outer segment phagosomes (rhodopsin, blue) in WT and *Abca4*$^{-/-}$ mouse RPE flatmounts at 1 h after light onset. Arrows: phagolysosomes. Scale bar: 2 µm. (**E**) Percent of phagosomes with either LAMP1, LAMP2, or both in WT and *Abca4*$^{-/-}$ mouse RPE. Mean ± SEM, n = 3 mice per genotype, ~3,000 outer segments/mice. (**F**) Representative immunofluorescence images of TFEB (red) in WT and *Abca4*$^{-/-}$ mouse RPE flatmounts at 5 h after light onset. Nuclei: blue (DAPI); Actin: gray (phalloidin). Scale bar:

5 μm. (**G**) Quantification of nuclear to cytoplasmic TFEB signal from (F). For B, C, and G: data are presented as Mean ± SEM. n.s., not significant, Welch's *t*-test. n = 3 mice/genotype. (**H**) Heatmap of TFEB target gene expression from RNAseq of WT and *Abca4*$^{-/-}$ mouse RPE harvested at 5 h after light onset (peak TFEB activation). Also see Figures S5 and S6. (**I**) Illustration of the three hierarchical roles of optineurin in tuning outside-in signaling to regulate daily outer segment phagocytosis and clearance by the RPE. See Discussion for details.

Key resources table

REAGENT or RESOURCE	SOURCE	IDENTIFIER
Antibodies		
Actin	Santa Cruz Biotechnology Inc., Dallas, Texas	Cat#Sc-1616
ATG16L1	Proteintech, Rosemont, IL	Cat#19812-1-AP
EEA1	Santa Cruz Biotechnology Inc., Dallas, Texas	Cat#sc-6415
FLAG (9A3)	Cell Signaling, Danvers, MA	Cat#8146
FOXO3	Proteintech, Rosemont, IL	Cat#10849-1-AP
GFP	MBL International Corporation, Woburn, MA	Cat#JM-3999-100
Lamin A/C	Proteintech, Rosemont, IL	Cat#10298-1-AP
LAMP1	Sigma-Aldrich, St. Louis, MO	Cat#L1418
LAMP2 (for pig RPE)	Bio-Rad, Hercules, CA	Cat#MCA2558
LAMP2 (for mouse RPE)	DSHB, Iowa, IA	Cat#GL2A7
LC3B	Sigma-Aldrich, St. Louis, MO	Cat#L7543
MYO6	Santa Cruz Biotechnology Inc., Dallas, Texas	Cat#sc-393558
MYO6	LSBio, Lynnwood, WA	Cat#LS-B13579-50
Optineurin	GeneTex Inc, Irvine, CA	Cat#GTX105447
RAB8	Origene, Rockville, MD	Cat#AB3176-200
Rhodopsin	Abcam, Cambridge, MA	Cat#ab229650
Rhodopsin C-terminus (clone 1D4)	Millipore, Burlington, MA	Cat#MAB5356
Rhodopsin N-terminus (clone 4D2)	Millipore, Burlington, MA	Cat#MABN15
α-tubulin	Santa Cruz Biotechnology Inc., Dallas, Texas	Cat#sc-53029
TFEB	Proteintech, Rosemont, IL	Cat#13372-1-AP
TOM20	Santa Cruz Biotechnology Inc., Dallas, Texas	Cat#sc-11415
TOM70	Abnova, Taipei, Taiwan	Cat#H00009868-B01P
β-Tubulin	Proteintech, Rosemont, IL	Cat#10094-1-AP
ZO-1	Developmental Studies Hybridoma Bank	Cat#R26.4C
DyLight™ 405 AffiniPure Fab Fragment Goat Anti-Mouse IgG2b	Jackson ImmunoResearch Laboratories Inc., West Grove, PA	Cat#115-477-187
Alexa Fluor secondary antibodies – various	ThermoFisher Scientific, Waltham, MA	
Bacterial and virus strains		
Premo Autophagy LC3B-GFP	ThermoFisher, Waltham, MA	Cat#P36235
Biological samples		
Primary porcine RPE	Lampire Biologicals	N/A
Chemicals, peptides, and recombinant proteins		

REAGENT or RESOURCE	SOURCE	IDENTIFIER
NativePAGE™ 4–16% Bis-Tris gel	Invitrogen, Waltham, MA	Cat#BN1004BOX
NativePAGE™ Sample Prep Kit	Invitrogen, Waltham, MA	Cat#BN2008
NativePAGE™ Running Buffer Kit	Invitrogen, Waltham, MA	Cat#BN2007
NativeMark™ Unstained Protein Standard	Invitrogen, Waltham, MA	Cat#LC0725
NE-PER Nuclear and Cytoplasmic Extraction Reagents	Thermo Scientific, Waltham, MA	Cat#78833
NuPAGE 4–12% Bis-Tris	Invitrogen, Waltham, MA	Cat#NP0336BOX
4X NuPAGE LDS sample buffer	Invitrogen, Waltham, MA	Cat#NP0007
10X NuPAGE Sample Reducing Agent	Invitrogen, Waltham, MA	Cat#NP0009
Phenylmethylsulfonyl fluoride (PMSF)	Tocris, Bristol, UK	Cat#4486
Protease Inhibitor Cocktail Set III, EDTA-Free	Millipore, Burlington, MA	Cat#539134
Intercept (PBS) Protein-Free Blocking Buffer	LI-COR, Lincoln, NE	Cat#927-90001
Revert™ 700 Total Protein Stain and Wash Solution Kit	LI-COR, Lincoln, NE	Cat#926-11015
SeeBlue Plus2 Pre-stained Protein Standard	Invitrogen, Waltham, MA	Cat#LC5925
Bovine Serum Albumin	Rockland Immunochemicals, Pottstown, PA	Cat#BSA-50
Calcium Chloride Dihydrate	Sigma-Aldrich, St. Louis, MO	Cat#C7902
DAPI (14.3 mM stock solution, used at 1:200)	Sigma-Aldrich, St. Louis, MO	Cat#D9542
Glucose	Sigma Aldrich, St. Louis, MO	Cat#G7528
HBSS	Corning, Corning, NY	Cat#21-023-CV
HEPES	ThermoFisher, Waltham, MA	Cat#15630080
Laemmli SDS-Sample Buffer	BioWorld, Dublin, OH	Cat#C995V98
Magnesium Chloride Hexahydrate	Sigma-Aldrich, St. Louis, MO	Cat#M2393
Paraformaldehyde (8%)	Electron Microscopy Sciences, Hatfield, PA	Cat#157-8
Phosphate Buffer Saline	ThermoFisher Scientific, Waltham, MA	Cat#BP665-1
10X RIPA buffer	Abcam, Cambridge, MA	Cat#ab156034
Saponin	Sigma-Aldrich, St. Louis, MO	Cat#84510
Sucrose	Sigma-Aldrich, St. Louis, MO	Cat#S0389
TrueBlack	Biotium, Fremont, CA	Cat#23007
VectaShield	Vector Laboratories, Burlingame, CA	Cat#H1000
Ciprofloxacin	Sigma-Aldrich, St. Louis, MO	Cat#17850-5G-F
DMEM	Corning, Corning, NY	Cat#10-013-CV
Fetal Bovine Serum (heat-inactivated)	American Type Culture Collection, Manassas, VA	Cat#30-2020
Non-essential amino acids (NEAA)	Corning, Corning, NY	Cat#25-025-CI
Penicillin-Streptomycin	Corning, Corning, NY	Cat#30-002-CI
0.25% Trypsin	Corning, Corning, NY	Cat#25-053-CI
2.5% Trypsin	Lonza, Walkersville, MD	Cat#17-160E
Opti-MEM	Gibco, ThermoFisher, Waltham, MA	Cat#31985-070
Rhodamine phalloidin	Cytoskeleton Inc., Denver, CO	Cat#PHDR1

REAGENT or RESOURCE	SOURCE	IDENTIFIER
Acti-stain 488 phalloidin	Cytoskeleton Inc., Denver, CO	Cat#PHDG1
CellMask Orange	Invitrogen, Waltham, MA	Cat#C10045
Lysotracker Red	Invitrogen, Waltham, MA	Cat#L7528
Mix-n-Stain™ CF®405 Dye Antibody Labeling Kit	Biotium, Fremont, CA	Cat#92272
MitoCDNB	Sigma-Aldrich, St. Louis, MO	Cat#SML2573
MLSI3	Gift from Haoxing Xu (University of Michigan, Ann Arbor, MI)	
Urolithin A	Toronto Research Chemicals, Toronto, Canada	Cat#U847000
Myo6 inhibitor (2,4,6-Triiodophenol, TIP)	Sigma-Aldrich, St. Louis, MO	Cat#137723
Critical commercial assays		
DC protein assay reagents	Bio-Rad, Hercules, CA	Cat#5000116
Duolink® In Situ Orange Starter Kit Mouse/Rabbit	Millipore-Sigma, Burlington, MA	Cat#DUO92102-1KT
Deposited data		
Bulk RNA sequencing data	This paper	https://www.ncbi.nlm.nih.gov/geo/query/acc.cgi?acc=GSE237293
Original western blots	This paper	DOI: 10.17632/n9dvxgncsm.1
Experimental models: Organisms/strains		
129S1/SvlmJ mice	Jackson labs	RRID:IMSR_JAX:002448 Strain #:002448
Abca4$^{-/-}$ mice (*Abca4tm1Ght/J*)	Jackson labs	RRID:IMSR_JAX:023725 Strain #:023725
Oligonucleotides		
Lamp2 forward AGCACAGTATTTCCTGGTGCT	Petkau et al. 2017 [63]	N/A
Lamp2 reverse CGACAGGAGTCAGGTTGTAAGTTAA	Petkau et al. 2017 [63]	N/A
Cln3 forward CCCTCGGTTGGATAGTCGGA	PrimerBank [64]	226423883c1
Cln3 reverse GCCTGGTTCCACATGGCTC	PrimerBank [64]	226423883c1
M6pr forward TGCTGGAGGACTGAACTGTTA	PrimerBank [64]	14916479a1
M6pr reverse GAGCCACCTCGTTCTTTGACT	PrimerBank [64]	14916479a1
Map1lc3b forward TTATAGAGCGATACAAGGGGGAG	PrimerBank [64]	13385664a1
Map1lc3b reverse CGCCGTCTGATTATCTTGATGAG	PrimerBank [64]	13385664a1
Mcoln1 forward CTGACCCCCAATCCTGGGTAT	PrimerBank [64]	16716463a1
Mcoln1 reverse GGCCCGGAACTTGTCACAT	PrimerBank [64]	16716463a1
Sqstm1 forward AGGATGGGGACTTGGTTGC	PrimerBank [64]	26324858a1
Sqstm1 reverse TCACAGATCACATTGGGGTGC	PrimerBank [64]	26324858a1
Tfeb forward CCACCCCAGCCATCAACAC	PrimerBank [64]	6755736a1
Tfeb reverse CAGACAGATACTCCCGAACCTT	PrimerBank [64]	6755736a1
18s forward ATGGCCGTTCTTAGTTGGTG	Farmer et al. 2017 [65]	N/A
18s reverse GAACGCCACTTGTCCCTCTA	Farmer et al. 2017 [65]	N/A

REAGENT or RESOURCE	SOURCE	IDENTIFIER
Recombinant DNA		
pOPTN-EGFP (Park *et al.*[66])	Addgene, Watertown, MA	Cat#27052
FLAG-OPTN	SinoBiological, Beijing, China	Cat#HG14478-NF
pE478G OPTN-EGFP (Turturro *et al.*[67])	Addgene, Watertown, MA	Cat#68848
pBMN mEGFP-OPTN(F178A) (Padman *et al.*[38])	Addgene, Watertown, MA	Cat#119681
OPTN(F178A)-EGFP	Cloned from plasmid above into EGFP-C1	N/A
EGFP-C1	Clontech (now Takara Bio USA, Mountain View, CA)	discontinued
TFEB-GFP (Roczniak-Ferguson *et al.*[68])	Addgene, Watertown, MA	Cat#38119
Scrambled shRNA	Origene, Rockville, MD	Cat#TR30015
FOXO3 shRNA GGGAACCTGTCCTACGCCGATCTGATCAC	Origene, Rockville, MD	N/A
Software and algorithms		
GraphPad Prism	GraphPad Prism®, La Jolla, CA	
Adobe Illustrator	Adobe, San Jose, CA	
Photoshop	Adobe, San Jose, CA	
Imaris	Bitplane, Concord, MA	
Microsoft Excel	Microsoft Corporation, Albuquerque, NM	
NIS Elements	Nikon, Melville, NY	
Other		
T25 culture flasks	Corning, Corning, NY	Cat#353108
MatTek dish (35mm)	MatTek Corporation, Ashland, MA	Cat#P35G-1.5-14-G